Available online at www.sciencedirect.com
ScienceDirect
Developmental Biology 306 (2007) 669–684
DEVELOPMENTAL BIOLOGY
www.elsevier.com/locate/ydbio

Zic2 and *Zic3* synergistically control neurulation and segmentation of paraxial mesoderm in mouse embryo

Takashi Inoue [a], Maya Ota [a], Katsuhiko Mikoshiba [b], Jun Aruga [a,*]

[a] *Laboratory for Comparative Neurogenesis, RIKEN Brain Science Institute, Wako-shi, Saitama 351-0198, Japan*
[b] *Laboratory of Developmental Neurobiology, RIKEN Brain Science Institute, Wako-shi, Saitama 351-0198, Japan*

Received for publication 10 August 2006; revised 4 April 2007; accepted 5 April 2007
Available online 12 April 2007

Abstract

Zic family zinc-finger proteins play various roles in animal development. In mice, five *Zic* genes (*Zic1–5*) have been reported. Despite the partly overlapping expression profiles of these genes, mouse mutants for each Zic show distinct phenotypes. To uncover possible redundant roles, we characterized *Zic2/Zic3* compound mutant mice. *Zic2* and *Zic3* are both expressed in presomitic mesoderm, forming and newly generated somites with differential spatiotemporal accentuation. Mice heterozygous for the hypomorphic *Zic2* allele together with null *Zic3* allele generally showed severe malformations of the axial skeleton, including asymmetric or rostro-caudally bridged vertebrae, and reduction of the number of caudal vertebral bones, that are not obvious in single mutants. These defects were preceded by perturbed somitic marker expression, and reduced paraxial mesoderm progenitors in the primitive streak. These results suggest that Zic2 and Zic3 cooperatively control the segmentation of paraxial mesoderm at multiple stages. In addition to the segmentation abnormality, the compound mutant also showed neural tube defects that ran the entire rostro-caudal extent (craniorachischisis), suggesting that neurulation is another developmental process where Zic2 and Zic3 have redundant functions.

Keywords: Zic; Compound mutation; Neurulation; Somitogenesis; Gastrulation

Introduction

Zinc finger proteins belonging to the Zic family play critical roles in animal development (reviewed in Herman and El-Hodiri, 2002; Aruga, 2004; Grinberg and Millen, 2005). The proteins contain a phylogenetically conserved zinc finger domain that is composed of tandem repeats of five C2H2 motifs. In mammals, there are five *Zic*-related genes — *Zic1*, *Zic2*, *Zic3*, *Zic4*, and *Zic5* — all of which have been characterized at least in part as to their expression profiles, molecular functions, and loss-of-function phenotypes (references in previously listed reviews). However, the relationships among the five mammalian Zic proteins in the developmental context are poorly understood. In a previous study, *Zic1* and *Zic2* were shown to control cerebellar development synergistically (Aruga et al., 2002a), but the other combinations of mammalian *Zic* genes have not been addressed yet.

Among the five mammalian *Zic* genes, *Zic2* and *Zic3* have critical roles in embryogenesis. In human, *ZIC2* causes holoprosencephaly (Brown et al., 1998), which is characterized by impaired development of the medial part of the forebrain. *Zic2* hypomorphic mutant mice show not only holoprosencephaly but also neural tube defects (NTDs) in both the rostral and caudal ends of the neural tube, abnormalities in retinal axon projection and axial and appendage skeletal patterning, and suppressed neural crest formation (Nagai et al., 2000; Elms et al., 2003; Herrera et al., 2003). In comparison, human *ZIC3* has been identified as a causal gene of X-linked heterotaxy (situs ambiguous) syndrome (Gebbia et al., 1997). Mouse *Zic3* mutants show abnormalities related to left–right axis determination and a variety of developmental abnormalities, such as malposition of the primitive streak, NTDs, axial skeletal patterning defects, and hypoplastic cerebellum (Carrel et al.,

Abbreviations: Bn, *Bent-tail*; ISH, in situ hybridization; NTD, neural tube defect; PSM, presomitic mesoderm; WMISH, whole-mount in situ hybridization.

* Corresponding author.
E-mail address: jaruga@brain.riken.jp (J. Aruga).

0012-1606/$ - see front matter © 2007 Elsevier Inc. All rights reserved.
doi:10.1016/j.ydbio.2007.04.003

2000; Klootwijk et al., 2000; Purandare et al., 2002; Aruga et al., 2004; Ware et al., 2006). The developmental abnormalities caused by deficiencies of *Zic2* or *Zic3* seem to partly overlap as regards the manifestation of NTDs and skeletal defects such as tail deformity. However, the rostro-caudal positions of NTDs and the types of tail deformity differ between *Zic2* and *Zic3* mutants, raising questions concerning their functional relationship in each developmental process.

Accumulating evidence provides a clear picture of the expression profiles of the two genes in mouse (Aruga et al., 1996; Nagai et al., 1997, 2000; Aruga et al., 2002a; Purandare et al., 2002; Brown et al., 2003; Elms et al., 2003, 2004; Inoue et al., 2004). Summarization of this literature suggests that *Zic2* and *Zic3* generally are expressed in partly overlapping, but distinct, manners. Although some comparative studies clearly revealed this point (Nagai et al., 1997; Elms et al., 2004; Inoue et al., 2004), some ambiguities remain. There also are similarities between *Zic2* and *Zic3* in terms of their molecular functions. They bind the same DNA target sequences, act as transcriptional activators in reporter gene assays (Mizugishi et al., 2001), and have common interacting proteins (Koyabu et al., 2001; Mizugishi et al., 2004). These similarities suggest that some of the roles of *Zic2* and *Zic3* in mammalian development are redundant.

While re-examining the expression profiles of *Zic2* and *Zic3* in mouse embryos, we found that the two genes are uniquely expressed during somitogenesis. Somites, which are transient epithelial spheres of paraxial mesoderm cells, give rise to metameric structures, such as vertebrae and ribs. Somites are synchronously generated from the anterior end of the unsegmented mesenchymal precursor tissue, called the presomitic mesoderm (PSM), in an anterior to posterior direction in a rhythmic fashion at regular spatiotemporal intervals. Somite formation periodically removes an unsegmented paraxial mesoderm from the PSM, and new mesodermal cells are continuously added on PSM posterior regions that include the primitive streak during gastrulation and the tailbud at later stages (Dubrulle and Pourquie, 2004). Before morphologic segmentation, a segmental prepattern characterized by segmental gene expression is established in the anterior PSM (Saga and Takeda, 2001; Pourquie, 2003; Rida et al., 2004). For instance, expression of mouse *Mesp2*, a bHLH transcription factor, is initially expressed in a segment-wide domain in the anterior PSM (Saga et al., 1997; Saga and Takeda, 2001). This initial segmental expression domain is defined by a molecular oscillator, called the "segmentation clock," which includes the Notch signaling pathway and *hairy/enhancer of split*-related transcription factors (Holley and Takeda, 2002; Maroto and Pourquie, 2001) and is related to the gradient of FGF and Wnt signaling in the posterior PSM (Galceran et al., 2004; Hofman et al., 2004; Kawamura et al., 2005). Although the involvement of *Zic* genes in somitogenesis is unknown, the expression pattern tempted us to examine their relevance to above processes.

To clarify the presumed redundant roles, we generated *Zic2/Zic3* mutant mice and analyzed their embryonic defects. Comparison of the phenotypes of the compound mutants with those of the single mutants indicated that *Zic2* and *Zic3* have common roles, both in segmentation of paraxial mesoderm and in neurulation.

Materials and methods

Animals

C57BL/6J and BALB/c mice were purchased from Nihon SLC (Shizuoka, Japan). Mice heterozygous for the *Zic2* "knock-down" mutation (*Zic2*^{tm1Jaru}, http://www.informatics.jax.org/) (Nagai et al., 2000) were backcrossed to C57BL/6J and BALB/c 12 or 13 times. These backcrossed mice then were used in subsequent matings. *Zic2* mutant mice were genotyped and maintained as described (Nagai et al., 2000; Aruga et al., 2002a). The spontaneous mutation in the *Bent tail* (*Bn*) (Garber, 1952) mouse was revealed to be a deletion of a region of the X chromosome including *Zic3* (*Zic3*^{Bn})(Carrel et al., 2000; Klootwijk et al., 2000). *Bn* mice were originally purchased from Jackson Laboratory (Bar Harbor, Maine, USA) and have been kept in a mixed C57BL/6J×BALB/c background. The phenotypes of *Bn* mice are very similar to that of *Zic3*-deficient mice generated by targeted mutation (Purandare et al., 2002; Aruga et al., 2004). Ware et al. (2006) described a variation in the gastrulation phenotypes of the *Zic3* knockout mice and classified them into four types in their study. We observed similar variances in the gastrulation phenotypes of *Zic3* mutants and confirmed that embryos representing each of the four types exist in the *Bn/Y* (*Zic3*$^{Bn/Y}$) or *Bn/Bn* (*Zic3*$^{Bn/Bn}$) E6.5–9.0 embryos. When we examined at E6.5–9.5, 32.5% (n=84) of the *Bn/Y* embryos showed no obvious morphologic abnormalities [type IV in Ware et al. (2006)]. *Zic2 kd/+ Zic3 Bn/Y* males were generated by mating *Zic3 Bn/+* females with *Zic2 kd/+* males. Crosses of viable *Zic2 kd/+ Zic3 Bn/+* females by *Zic2 kd/+* males generated double homozygous males (*Zic2 kd/kd Zic3 Bn/Y*). Animals were maintained by the Research Resource Center, RIKEN Brain Science Institute. All animal experiments were carried out in accordance with the guidelines for animal experiments in RIKEN. All efforts were made to minimize the number of animals used. Noon of the day on which vaginal plugs were first observed in the morning was defined as embryonic day 0.5 (E0.5). Staging criteria described for E6.5–7.5 embryos (Downs and Davies, 1993) were used to determine the stage of gastrulation of embryos. The genotype of the *Zic2* hypomorphic allele was determined (Nagai et al., 2000). Genotyping of the *Zic3* and *Zic3*^{Bn} alleles was performed as described (Klootwijk et al., 2000; Franke et al., 2003).

In situ hybridization, immunofluorescence, and histology

In situ hybridization (ISH) was performed essentially as described (Nagai et al., 1997). RNA probes for *Zic2* and *Zic3* were described previously (Nagai et al., 1997). RNA probes for *Fgf8*, *Foxa2*, *Mesp2*, *Mox1*, *Otx2*, *Paraxis*, *Pax1*, *Brachyury(T)*, and *Uncx4.1* were generated by RT–PCR; their sequences will be provided upon request. RNA probes for *Wnt3a* and *Pax3* were described by Takada et al. (1994) and Goulding et al. (1991), respectively. For E6.0–7.5 embryos, genotypes were identified after ISH by digestion of the embryos in a proteinase K-containing lysis buffer and subsequent PCR analysis. For

Fig. 1. Localization of mouse *Zic2* and *Zic3* mRNA and protein in early-stage mouse embryos. In all pictures, anterior is to the right, and all intact embryos are shown in lateral view except in panels G and P (dorsal view). The distributions of *Zic2* (A–I) and *Zic3* (J–R) mRNA are shown at E7.0 (A, J), E7.5 (B, C, K, L), E8.0 (D, E, M, N), E8.5 (F, G, O, P), E8.75 (H, Q), and E9.0 (I, R). Embryos were examined by ISH. Zic proteins were detected by immunofluorescence staining using anti-pan-Zic antibody (S–V) in E7.0 (S) and E7.5 (T) embryos in sagittal sections and in E8.0 (U) and E8.5 (V) embryos in transverse sections. The positions of the transverse sections are shown in panels B and F. Arrowheads in panels D–I and panels M, O–R indicate the expression of *Zic2* and *Zic3* in the anterior PSM and newly generated somites. al, allantois; ba, branchial arch; ch, chorion; fb, forebrain; e, eye; ec, embryonic ectoderm; ex, extraembryonic ectoderm; hb, hindbrain; hf, head fold; mes, embryonic mesoderm; nf, neural fold; ps, primitive streak; psm, presomitic mesoderm; r, rhombomere, s, somite; sc, spinal cord.

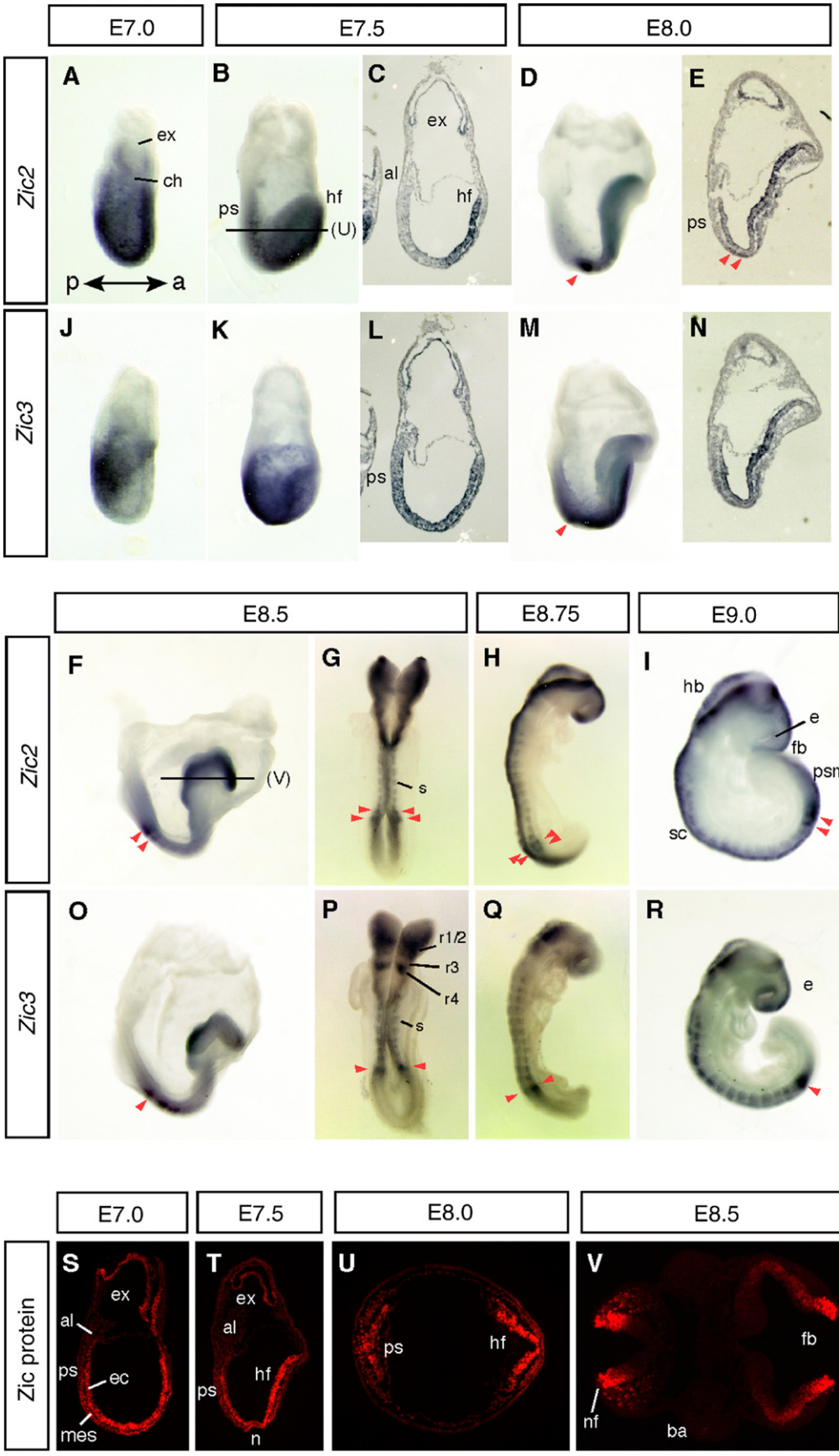
E7.0
E7.5
E8.0
Zic2
Zic3
A
B
C
D
E
J
K
L
M
N
ex
ch
p
a
hf
ps
(U)
al
E8.5
E8.75
E9.0
F
G
H
I
O
P
Q
R
(V)
s
hb
e
fb
psm
sc
r1/2
r3
r4
Zic protein
S
T
U
V
ec
mes
n
ba
nf

histological examination, specimens were fixed in either Bouin's solution or 4% paraformaldehyde, 0.1 M sodium phosphate (pH 7.4). After fixation, embryos were dehydrated through graded alcohols, embedded in paraffin, sectioned at a thickness of 8 to 10 μm, and stained with hematoxylin and eosin. Immunohistochemistry was performed as described previously (Aruga et al., 2002a). Embryos were excised, fixed in 4% paraformaldehyde in PBS at 4 °C overnight, cryoprotected in 30% sucrose in PBS overnight, and embedded in OCT compound; 6- to 10-μm cryosections were cut and examined

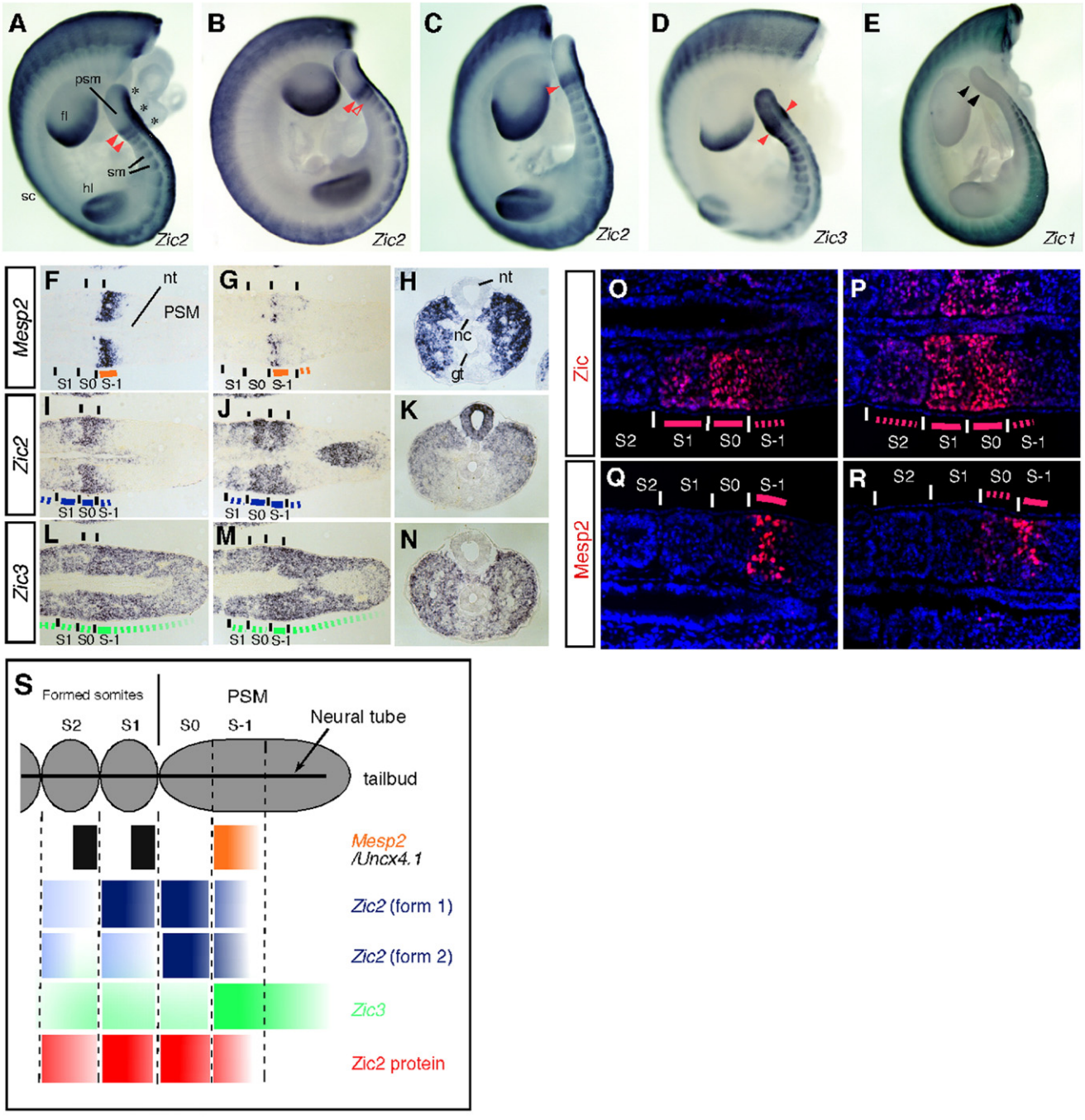

Fig. 2. Expression of *Zic2* and *Zic3* in PSM and somites at E10.5. (A–E) WMISH for *Zic2* (A–C), *Zic3* (D), and *Zic1* (E) mRNA. Lateral view of whole embryos. Expression of *Zic2* and *Zic3* in the anterior PSM and newly generated somites is indicated by arrowheads in panels A–D. The expression pattern of *Zic2* is variable in the anterior PSM and newly generated somites. Expression of *Zic2* in the tail dorsal neural tube is indicated by asterisks in panel A. (F–N) Expression analysis of *Mesp2*, *Zic2*, and *Zic3* in the tail at E10.5. Expression of *Mesp2* (F–H), *Zic2* (I–K), and *Zic3* (L–N) mRNA was compared by ISH of three sets of adjacent sections. (F, I, L) and (G, J, M) are sets of adjacent longitudinal sections through tail tip, respectively. (H, K, N) are transverse sections through S-1 region. Somites are numbered so that the newest somite is S1, the forming somite is S0, and the next somite to be formed is S-1, which is positive for *Mesp2* expression. fl, forelimb; gt, gut; hl, hindlimb; nc, notochord; nt, neural tube; psm, presomitic mesoderm; sc spinal cord; sm, somite. Solid and dotted lines indicate areas of enhanced and weak expression, respectively. (O–R) Distribution of Zic and Mesp2 proteins in the PSM and newly formed somites at E10.5. Immunopositive signals seem to mostly represent Zic2 protein at these stages. Zic (O, P) and Mesp2 (Q, R) proteins were detected by immunofluorescence labeling of two pairs of adjacent sections, (O, Q) and (P, R). Solid and dotted lines indicate regions of enhanced and weak expression, respectively. (S) Schematic drawing of expression domains of *Zic2* and *Zic3* mRNA, and Zic2 protein.

immunohistochemically. Fixed sections were washed three times with PBS and preincubated in PBS containing 5% normal donkey serum and 0.1% Triton X-100 for 30 min and then incubated in 1% normal donkey serum and 0.1% Triton X-100 with the primary antibodies. Anti-pan-Zic antibodies were generated by immunizing rabbits with glutathione *S*-transferase-Zic2 carboxy terminal region (amino acid number, 416–530 in NP_033600) and subsequent affinity purification at a company (MBL, Nagoya, Japan). The antibody primarily recognizes Zic2 protein, but also cross-reacts weakly to Zic1 and Zic3 in an immunoblot analysis (data not shown). The other primary antibodies used were: rabbit anti-Mesp2 (provided by Yumiko Saga) (Morimoto et al., 2005), mouse anti-165-kDa neurofilament (2H3, Developmental Studies Hybridoma Bank; DSHB), goat anti-Notch1 (Santa Cruz), rabbit anti-NICD (Notch intracellular domain) (Cell Signaling Technology), and rabbit anti-phosphohistone H3 (Upstate). For immunofluorescence detection of NICD and Mesp2, frozen sections were immersed in 0.01 M citrate buffer (pH 6.0), or Target Retrieval Solution (Dako), and autoclaved at 105 °C for 15 min to enable antigen retrieval (Tokunaga et al., 2004; Morimoto et al., 2005). To detect these antibodies, Cy3- (Jackson ImmunoResearch Laboratory), Alexa488-, and Alexa594-labeled secondary antibodies (Molecular Probes) were used. Fluorescently labeled preparations were imaged under an Olympus Fluoview FV300 confocal microscope or a Carl Zeiss Axioskop2 plus microscope equipped with an AxioCam color CCD camera. All images were analyzed with Adobe Photoshop CS software (Adobe Systems). Whole-mount immunohistochemical staining with 2H3 anti-neurofilament antibody was performed as described (Inoue et al., 2004). Skeletal analysis of fetuses and newborn animals was performed after staining with alcian blue and arizarin red staining (Hogan et al., 1994).

Cell proliferation analyses

Wild-type ($n=6$), *Zic3 Bn/Y* ($n=5$), and *Zic2 kd/+ Zic3 Bn/Y* ($n=4$) embryos were fixed at E7.75 and 8.5, and embedded in OCT compound. Tissue sections (7 μm) were subjected for immunofluorescence staining with anti-phosphohistone H3 antibody and nuclear staining with DAPI. The labeled cells were counted in four comparable sections per each embryo. Mitotic indices (percentage of cells undergoing mitosis) were calculated as percentages of the phosphohistone H3-positive nuclei among the DAPI-stained nuclei. At least, 16 sections from each genotype at each stage were evaluated to determine the mean percentages and the standard deviations. Statistical significance was assessed by *t*-test.

Results and discussion

Expression of Zic2 and Zic3 in early-stage embryos

We first performed a series of ISH to compare the expression profiles of *Zic2* and *Zic3* (Fig. 1). At E7.0 (mid to late streak stage), *Zic2* was expressed broadly in both the extra-embryonic and embryonic components of the egg cylinder (Fig. 1A). As development proceeded, *Zic2* expression increased, first in the anterior ectoderm and mesoderm of the headfold (Figs. 1B, C) and later in dorsal neural folds, somites (Figs. 1D–I), and segmenting trunk, with enhancement in a few caudal segments (arrowheads in Figs. 1D–I) of somite-stage embryos (E8.0–9.0). In contrast, *Zic3* transcripts were located more posteriorly in both ectoderm and mesoderm at the mid to late primitive streak stage (E7.0; Fig. 1J) and early neural fold stages (E7.5–8.0; Figs. 1K–N), and in the hindbrain regions (rhombomere [r] 1, 2, and 4) at later stages (E8.5–9.0; Figs. 1O–R). Similarly to *Zic2*, *Zic3* was expressed in the dorsal neural tube, somites, and the segmenting trunk, with enhancement in the caudal segments (arrowheads in Figs. 1M, O–R) in somite-stage embryos.

To characterize the distribution of Zic proteins at these stages, we conducted immunofluorescence staining (Figs. 1S–V). As judged by anti-Zic antibody, which originally raised against Zic2, but weakly cross reacts to Zic1 and Zic3, Zic proteins were located in the cell nuclei of the ectodermal and mesodermal cells of the primitive streak, headfold, and neural fold of the developing embryos. The distribution of the proteins corresponded to the region in which either *Zic2* or *Zic3* mRNA was detected, suggesting that there is no strong spatial difference in translation efficiency in these tissues. Therefore, in streak- to somite-stage embryos, expression overlapped throughout most of the neuroectoderm, with differing accentuation rostro-caudally (*Zic2*, stronger in the anterior; *Zic3*, stronger in the hindbrain and spinal cord-forming region), in the dorsal neural tube, and in some parts of the paraxial mesoderm.

Because expression of *Zic2* and *Zic3* occurred consistently in somites and the segmenting trunk of embryos from E8.0 through E11.5 (Fig. 1 and data not shown), we performed detailed examination of *Zic2* and *Zic3* expression in the tail (Fig. 2), in which the segmentation process has been well studied. As comparative markers, we used *Mesp2* mRNA and Mesp2 protein, whose differential expression represents various stages of somitogenesis (reviewed in Aulehla and Herrmann, 2004; Dubrulle and Pourquie, 2004; Saga and Takeda, 2001). We also examined expression of *Zic1* for comparison.

We detected *Zic2* expression in the somites, anterior PSM (arrowheads in Figs. 2A–C), and caudal end of the neural tube (asterisks in Fig. 2A) in E10.5 tails (Figs. 2A–C, I–J). Expression of *Zic2* in the PSM varied among the embryos examined. In 63% of E10.5 embryos (12 of 19), *Zic2* expression in the PSM and somite was detected as two distinct stripes (arrowheads in Figs. 2A, B). Comparison of the expression region of *Zic2* with that of *Mesp2*, which is expressed in the anterior portion of the prospective somite (S-1) (Saga et al., 1997; Takahashi et al., 2000) in adjacent section, revealed two stripes of *Zic2* mRNA corresponding to S0 (forming somite) and S1 (most newly formed somite) (Figs. 2F, I), and also expressed anterior part of S-1 weakly. Elsewhere, however, the expression of *Zic2* in S1 was weaker than in S0 (Fig. 2B, 2 of 19 embryos examined) or was detected as a single broad stripe (Fig. 2C, 5 of 19 embryos examined) in which the posterior half of the broad stripe corresponded to S-1 (demarcated by *Mesp2*) and the anterior to S0 (Figs. 2G, J). *Zic2* expression in segmented somites was weaker than in forming or newly generated somites but was still prominent, with slight enhancement in the anterior compartments (Figs. 2I–J). These variations may be better interpreted as changes in *Zic2* expression that are synchronous with the segmentation process, i.e., *Zic2* expression is initiated in S-1, is enhanced in the forming S0 somite, and is decreased at S1 and segmented somites (Fig. 2S).

In contrast to *Zic2*, *Zic3* expression in the tail was present as a single stripe throughout E8.0 to E11.5 (Fig. 1, and data not shown). At E10.5, *Zic3* expression in the tail occurred broadly throughout the PSM and somites but not in the neural tube, and appeared as a single stripe in the anterior PSM with a gradient to the posterior end (Figs. 2D, L, M). Comparison of the expression of *Zic3* with that of *Mesp2* revealed that the stripe of *Zic3* coincided with that of *Mesp2* (S-1; Figs. 2F, G, L, M, 17 of 20 embryos). In segmented somites, *Zic3* expression was

Table 1
Results of (*Zic2 Kd/+ Zic3 +/Y*)×(*Zic2 +/+ Zic3 Bn/+*) matings

Alleles		Collected frequency (%)				Expected frequency (%)
Zic2	Zic3	<E7.5	E7.5–9.5	E9.5–12.5	E12.5–18.5	
+/+	+/+ or Bn/+	21.9 (14/64[a])	26.4 (28/106[a])	23.5 (23/98[a])	28.4 (33/116[a])	25.0
+/+	+/Y	10.9 (7/64)	9.4 (10/106)	14.3 (14/98)	12.9 (15/116)	12.5
+/+	Bn/Y	9.4 (6/64)	10.4 (11/106)	10.2 (10/98)	14.7 (17/116)	12.5
Kd/+	+/+ or Bn/+	28.1 (18/64)	26.4 (28/106)	28.6 (28/98)	25.0 (29/116)	25.0
Kd/+	+/Y	15.6 (10/64)	17.9 (19/106)	15.3 (15/98)	13.8 (16/116)	12.5
Kd/+	Bn/Y	14.1 (9/64)	9.4 (10/106)	8.2 (8/98)	5.2 (6/116)	12.5

[a] Total embryos analyzed.

distributed evenly rostro-caudally (Figs. 2D, L, M). *Zic1* was not expressed in the PSM from E8.0 to E11.5 (Fig. 2E, and data not shown) but is abundantly expressed in more rostral somites and their derivatives (Nagai et al., 1997; Aruga et al., 1999). Antibody staining for Zic (Figs. 2O, P) and Mesp2 (Figs. 2Q, R) proteins also revealed that expression of Zic proteins is weak in anterior S-1 and strong in S0 and S1, and occasionally in S2. Examination of the *Zic2* mRNA and Zic protein in neighboring sections revealed that *Zic2* mRNA localization pattern was found to be mostly consistent with the immunopositive signals (Supplemental Fig. 1A, C). However, we observed bands of Zic protein in S-1, S0, S1, and S2 while the *Zic2* mRNA was strong in S-1, S0 and S1, but diminished in S2. This result suggests that the *Zic2* mRNA disappears earlier than the protein. Similar difference was observed between *Mesp2* mRNA and protein in the neighboring sections (Supplemental Fig. 1D, E). *Mesp2* mRNA was predominantly detected in S-1 while Mesp2 protein was both in S-1 and S0 as reported by Morimoto et al. (2005). Collectively, the results of the expression pattern analysis raised a possibility that *Zic2* and *Zic3* act together in the neuroectoderm, primitive streak, somites, and anterior PSM.

Zic2 and Zic3 cooperatively control neurulation

To characterize the embryonic defects of *Zic2*/*Zic3* compound mutants, two types of mating were carried out. One was a *Zic2 kd/+*×*Zic3 Bn/+* intercross to generate a heterozygous *Zic2* hypomorphic allele together with nullizygous *Zic3* (*Zic2 kd/+ Zic3 Bn/Y*) (Table 1), and the other was a *Zic2 kd/+ Zic3 +/Y*×*Zic2 kd/+ Zic3 Bn/+* intercross to generate the homozygous *Zic2* hypomorphic allele together with nullizygous *Zic3* (*Zic2 kd/kd Zic3 Bn/Y*) (Table 2). E6.5–18.5 embryos were harvested and genotyped by PCR.

We first characterized *Zic2 kd/+ Zic3 Bn/Y* embryos. By the end of embryonic development, most of the *Zic2 kd/+ Zic3 Bn/Y* embryos had been resorbed (Table 1, and data not shown). However, several attempts to collect surviving *Zic2 kd/+ Zic3 Bn/Y* embryos until E16–17.5 were successful ($n=6$). We found that 4 of the 6 *Zic2 kd/+ Zic3 Bn/Y* embryos at these stages showed marked NTD from the midbrain to the caudalmost region (craniorachischisis) (Figs. 3C, D), whereas NTD restricted to caudal or midbrain–hindbrain regions occurred in *Zic2 kd/kd* (Fig. 3A) or *Zic3 Bn/Y* (Fig. 3B) embryos, respectively, as described previously (Klootwijk et al., 2000; Nagai et al., 2000). The neurulation abnormalities could be traced back to E8.5–9.5 (Fig. 3E). At E9.5, *Zic3 Bn/Y* embryos showed growth retardation, slight rotation defects, and NTD in the hindbrain region. The frequency of hindbrain NTD was 29% (7 of 24) in E9.5–18.5. In contrast, 42% (5 of 12) *Zic2 kd/+ Zic3 Bn/Y* embryos at E9.0–10.5 showed craniorachischisis extending from the midbrain to the caudalmost region (Figs. 3E–G), and 6 of the 12 embryos showed more severe defects that precluded evaluation of neurulation (Figs. 7J and 9, C, F). Therefore, the severity of NTD was strongly enhanced in *Zic2 kd/+ Zic3 Bn/Y* in comparison with that in the single mutants. Besides NTD, *Zic2 kd/+ Zic3 Bn/Y* embryos also showed shortened rostro-caudal body length and dilated heart morphology (5 of 12 embryos at E9.0–10.5), compared with those in wild-type and *Zic3 Bn/Y* littermates. As a consequence, these results suggest that *Zic2* and *Zic3* commonly regulate neural

Table 2
Results of (*Zic2 Kd/+ Zic3 +/Y*)×(*Zic2 kd/+ Zic3 Bn/+*) matings

Alleles		Collected frequency (%)				Expected frequency (%)
Zic2	Zic3	<E6.5	E6.5–7.5	E7.5–8.5	>E8.5	
+/+	+/+ or Bn/+	9.4 (6/64[a])	10.3 (12/116[a])	12.2 (16/106[a])	17.7 (17/96[a])	12.5
+/+	+/Y	6.3 (4/64)	8.6 (10/116)	7.3 (9/106)	10.4 (10/96)	6.25
+/+	Bn/Y	9.4 (6/64)	6.0 (7/116)	8.5 (8/106)	7.3 (7/96)	6.25
Kd/+	+/+ or Bn/+	21.9 (14/64)	28.4 (33/116)	24.4 (30/106)	24.0 (23/96)	25.0
Kd/+	+/Y	14.1 (9/64)	10.3 (12/116)	14.6 (11/106)	16.7 (16/96)	12.5
Kd/+	Bn/Y	15.6 (10/64)	11.2 (13/116)	10.9 (10/106)	5.2 (5/96)	12.5
Kd/Kd	+/+ or Bn/+	9.4 (6/64)	12.9 (15/116)	11.0 (13/106)	10.4 (10/96)	12.5
Kd/Kd	+/Y	7.8 (5/64)	6.9 (8/116)	7.3 (5/106)	8.3 (8/96)	6.25
Kd/Kd	Bn/Y	6.3 (4/64)	5.2 (6/116)	3.7 (4/106)	0 (0/96)	6.25

[a] Total embryos analyzed.

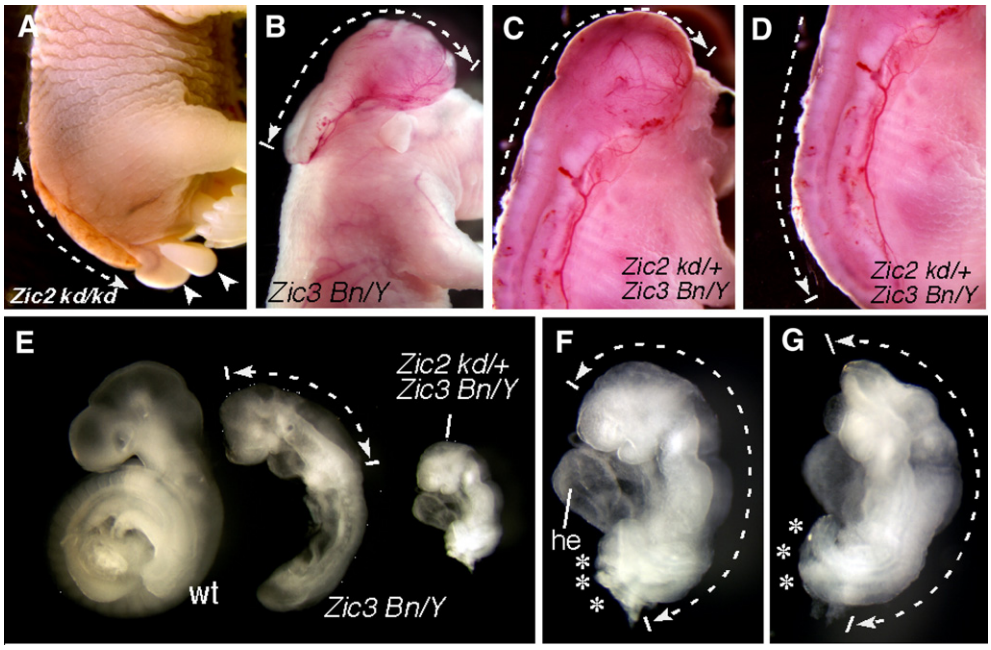

Fig. 3. Defects of neural tube closure in *Zic2 kd/kd*, *Zic3 Bn/Y*, and *Zic2 kd/+ Zic3 Bn/Y* mutants. (A–D) Dorso-lateral view of *Zic2 kd/kd* (A), *Zic3 Bn/Y* (B), and *Zic2 kd/+Zic3 Bn/Y* (C–D) E17.5–18.5 embryos. Lumbar (A), midbrain to hindbrain (B), and midbrain to lumbar (C–D) regions are affected in *Zic2 kd/kd*, *Zic3 Bn/Y*, and *Zic2 kd/+ Zic3 Bn/Y* embryos, respectively. Regions of neural tube defects are indicated by dashed lines. Curly tail of the *Zic2 kd/kd* is indicated by arrowheads in panel A. (E) Lateral view of wild-type, *Zic3 Bn/Y*, and *Zic2 kd/+ Zic3 Bn/Y* embryos at E9.5. (F, G) Lateral (F) and dorsal (G) views of the *Zic2 kd/+ Zic3 Bn/Y* embryos at E9.5. Abnormal and truncated morphology of the tail region is indicated by asterisks. The embryo also appears to show rotation defects. he, heart.

tube closure of the cervical to thoracic region. Together with previous results (Nagai et al., 2000; Klootwijk et al., 2000), it became clear that mouse *Zic2* and *Zic3* are essential for the neural tube closure at any rostro-caudal levels. It is possible that *Zic5* also coordinately controls the neurulation with *Zic2* and *Zic3*, considering its overlapping expression and the NTD phenotype in *Zic5* mutant (Inoue et al., 2004).

Skeletal patterning defects in Zic2/Zic3 compound mutant mice

We next examined the skeletal phenotypes of surviving *Zic2 kd/+ Zic3 Bn/Y* embryos at E16–17.5 and compared them with those of wild-type, *Zic2 kd/kd*, and *Zic3 Bn/Y* embryos (Fig. 4). *Zic2 kd/+ Zic3 Bn/Y* embryos were easily identified because they showed shortened body length and abnormally bent and short tails (Fig. 4D) compared with those of wild-type (Fig. 4A), *Zic2 kd/kd* (Fig. 4B) and *Zic3 Bn/Y* (Fig. 4C) embryos. These defects were observed in all (6 of 6) *Zic2 kd/+ Zic3 Bn/Y* embryos at this stage; they were also apparent in preskeletal cartilage at E14.5 (4 of 4 embryos, data not shown). Quantitative analysis revealed that the shortening of the body was due to a decrease in the number of vertebrae (Fig. 4E). The reduction was strong in the tail region but weak in the cervical, thoracic, and lumbar regions. The size of the vertebral bodies was comparable, except in the tail compartment (Fig. 5). Whereas the most affected embryos were *Zic2 kd/+ Zic3 Bn/Y*, *Zic2 kd/kd* and *Zic3 Bn/Y* embryos also showed significant decreases in the number of vertebrae in the tail region (Figs. 4B, C, E); *Zic2 kd/kd* embryos also had curly tails, whereas those of *Zic3 Bn/Y* embryos were kinked.

Detailed examination of the defects in the axial skeleton revealed that the disorganization extended along the entire rostro-caudal axis in *Zic* mutants at E16.5–17.5 (Fig. 5; Table 3). Defects were localized dorsally in the vertebral arch and ventrally in the vertebral bodies, ribs, and sterni, indicating that almost all axial skeletal bones were more or less affected. In *Zic2 kd/kd* embryos, vertebral arches were frequently fused to the adjacent ones in the cervical and thoracic regions (Fig. 5B). The vertebral arches were absent in the region of the caudal NTD (spina bifida), and the arch rudiments were fused with rostro-caudally adjacent ones throughout the NTD region (Fig. 5F). In addition, vertebral bodies were occasionally asymmetrically malformed (hemivertebrae, open arrowhead in Fig. 5B) and rostro-caudally fused (open arrowheads in Fig. 5F) in these regions. In the tail region, the dorsal parts of the vertebral bodies were fused together (11 of 12 *Zic2 kd/kd*, Fig. 5N) to form a "curly tail".

Skeletal abnormality in *Zic3 Bn/Y* embryos was milder than that of *Zic2 kd/kd*. Rostro-caudal fusion of the vertebral arches occurred only in the cervical and thoracic regions (Fig. 5C; Table 3, and data not shown). In the tails of *Zic3 Bn/Y* embryos, the vertebral bodies were asymmetrically aligned along both the dorsoventral and left–right axes, but they were rarely fused to each other (Figs. 5K, O; Table 3). We speculated that these differences may underlie the differences in tail phenotypes between *Zic2 kd/kd* and *Zic3 Bn/Y* embryos [i.e. *Zic2 kd/kd* curly tail (Nagai et al., 2000); *Zic3 Bn/Y* kinky tail (Carrel et al., 2000; Klootwijk et al., 2000)]. Another *Zic2*-hypomorphic mutant, *Zic2 ku/ku*, and *Zic3* knockouts also show curly and kinky tail phenotypes, respectively (Purandare et al., 2002;

Elms et al., 2003), confirming that these tail phenotypes are inherent to the loss of Zic2 and Zic3 functions.

As expected, *Zic2 kd/+ Zic3 Bn/Y* embryos showed more severe skeletal defects than did *Zic2 kd/kd* and *Zic3 Bn/Y* (Figs. 5D, H, L, P, T; Table 3). The vertebral arch rudiments were fused throughout the cervical to lumbar regions along the NTD (Figs. 5D, H), and asymmetrical malformation and rostro-caudal fusion of the vertebral bodies occurred frequently at all rostro-caudal levels (open arrowheads in Figs. 5D, H, and arrowheads in Figs. 5L, P). Vertebrae were fused strongly to each other, particularly in the tail region (Figs. 5L, P). The deformation was also observed in the rib and sternebrae, in which rostro-caudal position of the proximal ribs were asymmetric (Fig. 5T). These synergistic effects of *Zic2 kd* and *Zic3 Bn* mutations on skeletal deformation may reflect the redundant functions of *Zic2* and *Zic3*.

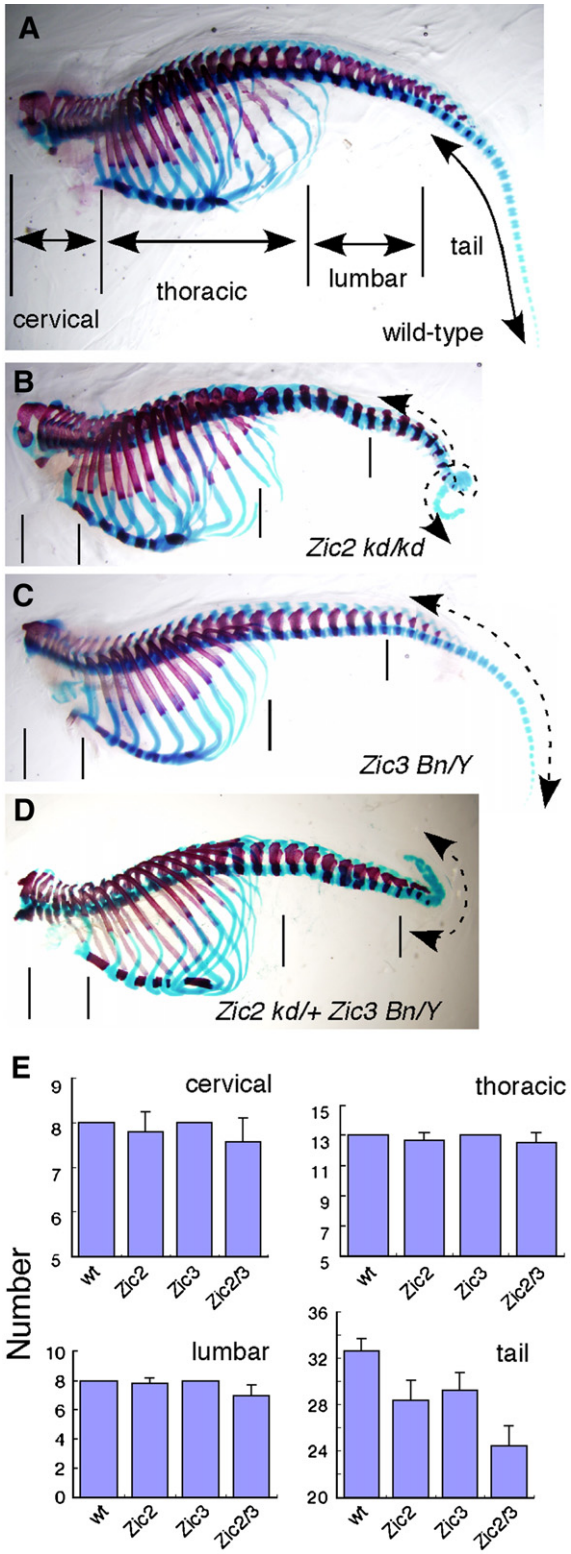

Fig. 4. Loss of *Zic* genes results in truncation of the body axis. Distribution of skeletal malformations at E17.5. (A–D) Lateral view of the axial skeleton (red, bones; blue, cartilage) of wild-type (A), *Zic2 kd/kd* (B), *Zic3 Bn/Y* (or *Zic3 Bn/Bn*) (C), and *Zic2 kd/+ Zic3 Bn/Y* (D) mutant mice. Dashed arrows indicate altered morphologies of the tail with decreased number of the vertebral bones. Wild-type control animals ($n=15$) rarely show any of the defects observed in mutant mice. (E) Decreased number of vertebral bones in *Zic* mutant mice. E16.5–17.5 (*Zic2 kd/+ Zic3 Bn/Y*) ($n=6$), *Zic2 kd/kd* ($n=8$), *Zic3 Bn/Y* ($n=12$), and wild-type ($n=7$) embryos were analyzed. We counted the vertebrae in the cervical, thoracic, lumbar, and tail regions (double arrows in panel A). *Zic2 kd/+ Zic3 Bn/Y* showed fewer caudal vertebral bones, and this difference was not so strong in either *Zic2* or *Zic3* single mutants.

Skeletal abnormalities are also found in *Zic1*-deficient mice (Aruga et al., 1999). In *Zic1*−/− embryos, the defects in the vertebral arch can be traced back to a disturbance in metameric cartilaginous condensation of the dorsal sclerotome cells. In *Zic1*-deficiency, early rostro-caudal specification of the somites and differentiation of the somites into sclerotome, myotome, and dermomyotome occur properly. Therefore, dorsal skeletal defects, such as deformities of vertebral arches like those in *Zic2 kd/kd*, *Zic3 Bn/Y*, and *Zic2 kd/+ Zic3 Bn/Y* embryos, could occur by a similar mechanism, considering the similar expression of *Zic1* in the dorsal spinal cord (Nagai et al., 1997; Aruga et al., 1999). However, the axial truncation and frequent asymmetrical and rostro-caudal malformation of the axial skeleton in *Zic2*, *Zic3*, and *Zic2/Zic3* mutants need alternative explanations, because these defects rarely are found in *Zic1*−/− embryos (Aruga et al., 1999). Because *Zic2* and *Zic3* are expressed strongly in undifferentiated PSM and S-1 and S0 somites, where *Zic1* is not expressed (Fig. 2E), we hypothesized that not only sclerotome differentiation but also the initial generation or patterning of the somites could be disturbed in *Zic2*, *Zic3*, and *Zic2/Zic3* compound mutants.

Somitogenesis is disorganized in Zic2 kd/kd and Zic3 Bn/Y embryos

To test whether *Zic2* and *Zic3* play roles in somite segmentation or patterning, we next analyzed somitogenesis in *Zic2 kd/kd* and *Zic3 Bn/Y* embryos (Fig. 6). First, we examined *Zic2 kd/kd* embryos. When examined at E9.5–12.5, *Zic2 kd/kd* were distinguishable from their littermates by caudal spina bifida and dorsally curved tails after E11.5 (Figs. 6A, C, S). In *Zic2 kd/kd* embryos, stripes of *Uncx4.1*, which is a marker for the posterior compartment of each somite, were frequently irregular along the rostro-caudal axis at E11.5 (6 of 6 embryos, arrowheads in Fig. 6C). The disturbance involved

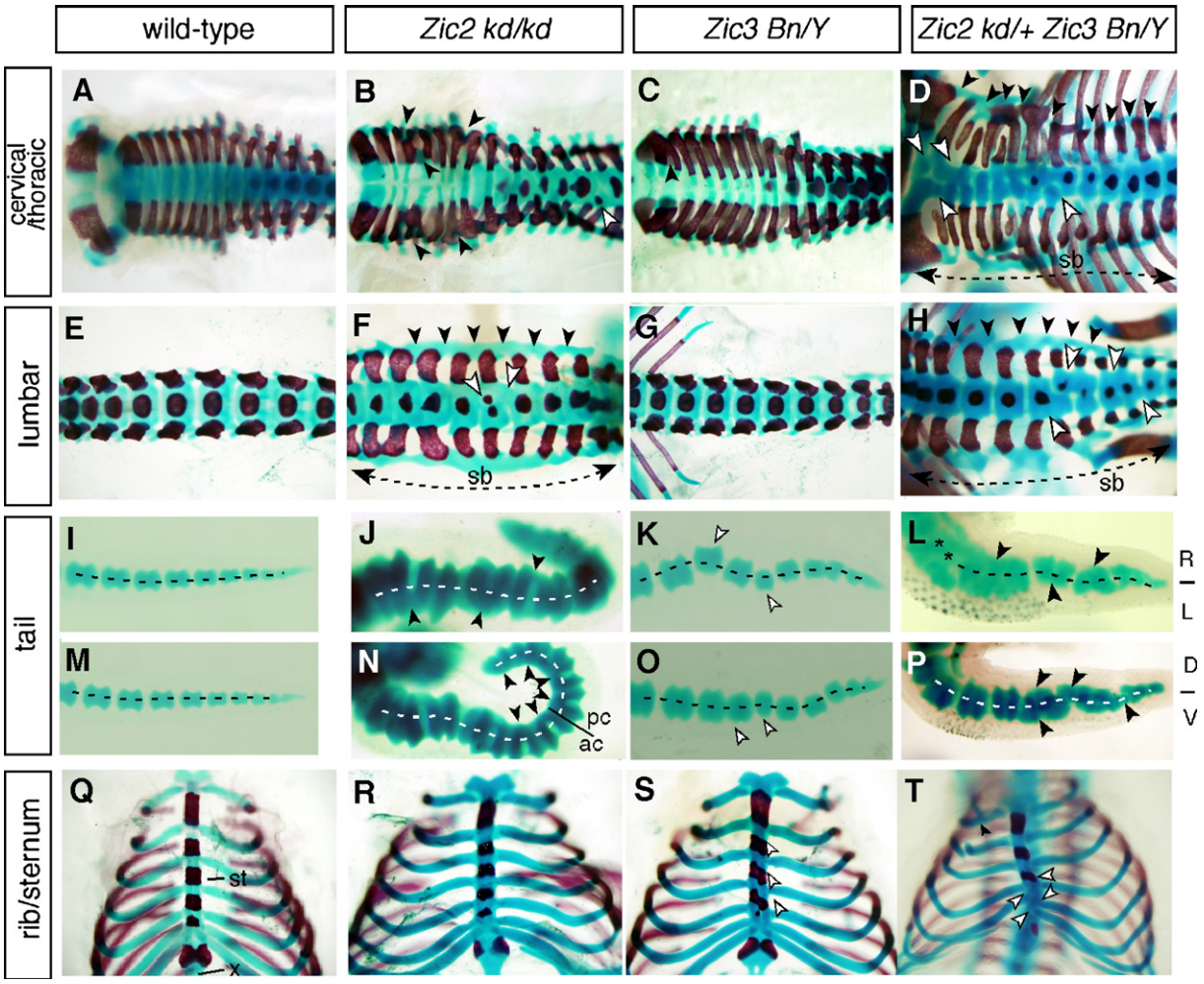

Fig. 5. Skeletal defects in *Zic2 kd/kd*, *Zic3 Bn/Y*, and *Zic2 kd/+ Zic3 Bn/Y* mutant mice. Skeletal staining (red, bones; blue, cartilage) for wild-type (A, E, I, M, Q), *Zic2 kd/kd* (B, F, J, N, R), *Zic3 Bn/Y* (C, G, K, O, S), and *Zic2 kd/+ Zic3 Bn/Y* (D, H, L, P, T) embryos at E17.5. Dorsal (A–L) or lateral (M–P) views of the vertebral columns. Cervical to upper thoracic (A–D), lumbar (E–H), tail (I–P). (Q–T) Ventral view of thoraxes. Anterior is to the left (A–P) or the top (Q–T). Regions of the neural tube closure defects (spina bifida, sb) are indicated by dashed arrows. Dashed lines indicate midline of the tails along the left–right and dorsoventral axes. Abnormalities of the skeletal components along the anterior–posterior axis, including fusion of the vertebral columns, vertebral arches, and laminae are indicated by closed arrowheads. Left–right asymmetric skeletal structures, including asymmetric morphologies of vertebral bodies and sternobrae and one-sided fusion of the vertebral bodies are indicated by open arrowheads. ap, anterior compartment of the somite; D, dorsal; V, ventral; L, left; pc, posterior compartment of the somite; R, right; sb, spina bifida; st, sternabrae; x, xiphoid process.

abnormal intrusion of *Uncx4.1*-positive cells into the anterior compartment, especially in dorsal somites (asterisks in Figs. 6F, G, I and Supplemental Fig. 2C). Histological examination revealed that the *Uncx4.1* stripes were partially close to each other in the thoracic region (Fig. 6F), and were continuous in the dorsal region in the curved parts of the tail region (Figs. 6G, I and Supplemental Fig. 2C). In an neighboring section, a somite anterior compartment marker, *Tbx18* (Kraus et al., 2001; Bussen et al., 2004), was not expressed in the region where ectopic *Uncx4.1* expression was observed (Supplemental Fig. 2D), suggesting the transformation of the anterior compartment into the posterior one or an intrusion of the posterior compartment into the anterior. Consistent with these observations, immunohistochemical detection of neurofilament (Dodd et al., 1988) at E10.5 revealed either lost or irregular arrangement of ganglia and spinal nerve axons in *Zic2 kd/kd* (Fig. 6K, and data not shown). The segmental pattern disturbance was also indicated by molecular markers for somite derivatives, such as *Pax1* (sclerotome, Deutsch et al., 1991), *Pax3* (dermomyotome, Goulding et al., 1994), and *Paraxis* (sclerotome and dermomyotome, Burgess et al., 1995) (Supplemental Fig. 2H–J). However, the results also suggested that the differentiation into these components was not severely impaired.

The somitic defects of *Zic3 Bn/Y* seemed milder than those of *Zic2 kd/kd*. *Uncx4.1* signals in *Zic3 Bn/Y* were weak, and both *Uncx4.1*-positive and -negative stripes were thinner in some embryos (6 of 14 *Zic3 Bn/Y* or *Zic3 Bn/Bn* embryos; Figs. 6L, N, O). The irregular stripe pattern seen in *Zic2 kd/kd* embryos was rare but was significantly detected in *Zic3 Bn/Y* (1 of 6 *Zic3 Bn/Y* embryos; asterisk in Fig. 6Q).

Recently, it was suggested that somite boundary is generated by suppression of Notch activity by Mesp2 (Morimoto et al.,

Table 3
Distribution and frequency of skeletal malformations in *Zic2 kd/kd*, *Zic3 Bn/Y*, and *Zic2 Kd/+ Zic3 Bn/Y* mutant at E16.5–17.5

	Zic2 kd/kd ($n=11$)	*Zic3 Bn/Y* ($n=12$)	*Zic2 Kd/+ Zic3 Bn/Y* ($n=6$)
Cervical (C1–C7)			
Fusion of vertebral arch	0.91	0.33	–
Fusion of vertebral column	0.18	–	0.5
Asymmetric vertebral bodies	0.09	–	0.33
Thoracic (T1–13)			
Fusion of vertebral arch	0.91	0.33	–
Fusion of vertebral column	0.18	–	0.5
Fusion of ribs	0.36	0.11	0.67
Asymmetric vertebral column	0.45	–	0.33
Asymmetric sternum	0.36	0.67	0.33
Split vertebral bodies	0.27	–	–
Lumber (L1–L6, S1–S4)			
Fusion of vertebral bodies	0.13	–	0.33
Asymmetric vertebral column	0.09	–	0.33
Split vertebral bodies	0.25	–	–
Tail (Ca1∼)			
Fusion of vertebral column	1.00	–	1.00
Asymmetric vertebral column	0.91	0.91	1.00

2005). We therefore examined the distributions of Notch1 and activated Notch1 proteins in the *Zic2 kd/kd* PSM at E10.5–12.5 (Figs. 6W, X–AA). There were no clear differences between *Zic2 kd/kd* mutants ($n=18$) and their wild-type littermates ($n=22$) in either Notch1 (Fig. 6W) or activated Notch1 (NICD, in Figs. 6X–AA) immunofluorescence staining. Examination of other markers for anterior PSM, *EphA4* (Nieto et al., 1992; Nakajima et al., 2006) and *Mesp2* also revealed no clear differences between the mutants and wild-type (Supplemental Fig. 3A–B, D–E; and data not shown). In addition, in the neighboring section, correct stripe of *Uncx4.1* expression in the newly formed somites indicated that anterior–posterior somite polarity was normally specified in *Zic2 kd/kd* mutant (Supplemental Fig. 3F).

Besides the segmentation anomaly, *Zic2 kd/kd* mutants had slightly enlarged tailbuds when examined at E11.5–12.5 (asterisks in Fig. 6T). Histological sections through this region revealed disorganized cellular condensation in a continuous tissue from caudal neural tube (arrowheads in Fig. 6V). Together with the strong *Zic2* expression in the caudal end of the neural tube, this phenotype may reflect a role of *Zic2* in tail neurogenesis.

Segmentation and mesodermal patterning defects in the Zic2/Zic3 mutants

The phenotypes of the *Zic2* and *Zic3* single-mutant somites described above indicate that *Zic2* and *Zic3* have a role in somitogenesis. To reveal their possible synergy, we next examined the somite defects of *Zic2 kd/+ Zic3 Bn/Y* embryos. When examined at E8.5 (Fig. 7C) and E9.5 (Figs. 7F, G, J), *Zic2 kd/+ Zic3 Bn/Y* embryos showed a deficit in posterior development (Figs. 3E–G and 7C, F, G). Body lengths were shortened, and *Uncx4.1* transcripts were weakly and irregularly distributed in *Zic2 kd/+ Zic3 Bn/Y* embryos (Figs. 7F–G). The *Uncx4.1*-expressing somites were reduced in number, and the stripes of *Uncx4.1* expression were weaker and thinner in *Zic2 kd/+ Zic3 Bn/Y* embryos than in *Zic3 Bn/Y* embryos, suggesting lack of expansion of the somitic mesoderm. In addition, we noted that several *Zic2 kd/+ Zic3 Bn/Y* showed bilateral somite defects at E8.5–9.5, which was revealed by asymmetric *Uncx4.1* expression (inset in Fig. 7F). Expression of a mesodermal marker, *Brachyury*(*T*), was abnormally weak in the *Zic2 kd/+ Zic3 Bn/Y* PSM (Figs. 7C, F, G). *Mox1* is expressed in all cell types of somites, with enhancement in the caudal half, and in the anterior PSM in wild-type embryos at E9.5 (Fig. 7H; Candia et al., 1992). However, in *Zic3 Bn/Y* embryos, the *Mox1* stripe was slightly weaker but regular (Fig. 7I and data not shown). By contrast, *Mox1* signals appeared irregular, and without clear segmentation, in *Zic2 kd/+ Zic3 Bn/Y* embryos (arrowheads in Fig. 7J).

The analyses of *Zic2 kd/+ Zic3 Bn/Y* also indicated that PSM was present in the combined mutant, but the size was smaller than those of wild-type and *Zic3*-single mutant (Figs. 7C, F, G, J, 8G, and 9C, F). To determine if the cell proliferation is affected in the combined mutant, we examined the mitotic frequencies in the primitive streak in wild-type, *Zic3 Bn/Y*, and *Zic2 kd/+ Zic3 Bn/Y* embryos at E7.75 and E8.5, using a mitotic marker phospho-histone H3 (phospho-H3) (Fig. 8). As a result, primitive streak of *Zic2 kd/+ Zic3 Bn/Y* contained fewer phospho-H3-positive cells in the mesodermal layers through these stages (Figs. 8C, F), and the mitotic indices were significantly lower than that of wild-type and *Zic3 Bn/Y* at both stages (Figs. 8H, I). The mitotic indices of the overlying ectoderm were also reduced, but were not significantly differ among the three genotypes (Figs. 8H, I). As another possible explanation for the hypoplasticity of the PSM, change in the cell death frequency was possible. However, we did not see significant differences of the cell death frequency among the three genotypes (not shown). Collectively, these results suggested that *Zic2* and *Zic3* have a redundant function in promoting the cell proliferation of PSM progenitor cells.

In relation to the reduced proliferation of the early mesodermal cells, *Zic2 kd/+ Zic3 Bn/Y* embryos showed altered expression of some marker genes. *Wnt3a* (Takada et al., 1994) and *Fgf8* (Dubrulle et al., 2001) expression was generally reduced in their sizes (Figs. 9C, F, respectively). Not only area but also staining intensity was diminished for *Wnt3a* signals [43% of *Zic2 kd/+ Zic3 Bn/Y* mutants ($n=9$), arrowheads in Fig. 9F]. These results indicate that differentiation of mesodermal tissue may also be impaired in *Zic2 kd/+ Zic3 Bn/Y* mutants. The finding is important because *Brachyury*, *Wnt3a*, and *Fgf8* play crucial roles in mesodermal development.

Finally, we sought to analyze somite-related abnormalities of *Zic2 kd/kd Zic3 Bn/Y* embryos. However, the *Zic2 kd/kd Zic3 Bn/Y* embryos showed early embryonic lethality, and we failed to collect any embryos later than E8.5 (Table 2). The three *Zic2 kd/kd Zic3 Bn/Y* embryos that we obtained at E8.5 showed poor development of somitic structures (Fig. 9G). These data also support the idea that at least one allele of *Zic2* or *Zic3* is

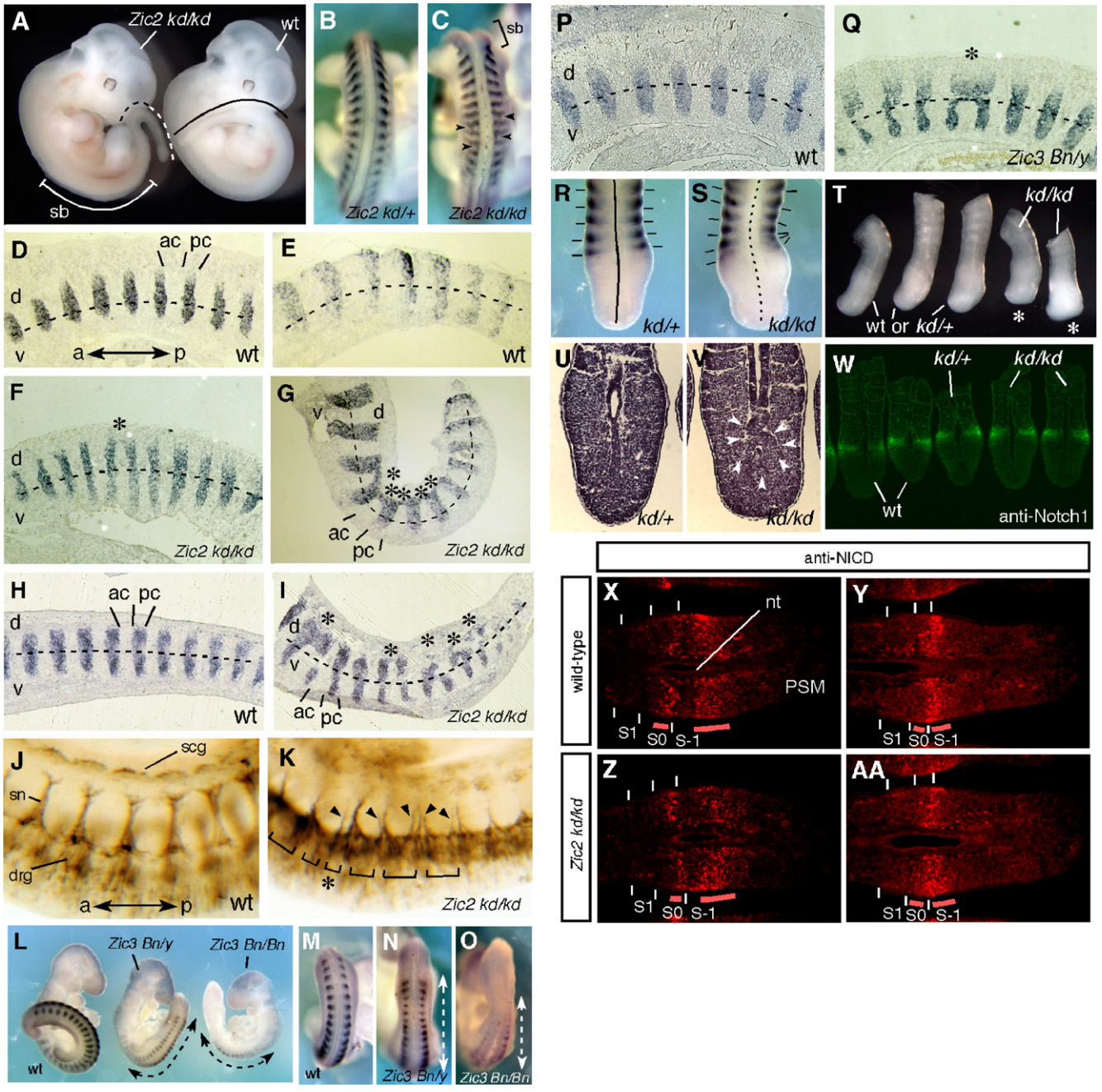

Fig. 6. Somite structures are disrupted in *Zic2* and *Zic3* mutant mice. (A) *Zic2 kd/kd* (left) and wild-type (right) embryos at E12.5. White line indicates open neural tube (spina bifida). Dashed line indicates the dorsally curled tail in *Zic2 kd/kd* in comparison to wild-type tail region (black line). (B, C, R, S) WMISH with somite posterior compartment marker, *Uncx4.1* RNA probes at E11.5 *Zic2 kd/+* (B, R) and *Zic2 kd/kd* (C, S). In the *Zic2 kd/kd* embryo (C), *Uncx4.1* expression was partly diffused (arrowheads in panel C), suggesting the disturbance of the anterior–posterior polarity of somite. sb, spina bifida. (D–I) ISH with *Uncx4.1* RNA probes at E11.5 (D–G) and E12.5 (H–I) in wild-type (D–E, H) and *Zic2 kd/kd* (F–G, I) embryos in longitudinal sections through thoracic (D, F) and tail regions (E, G, H, I). Fusion of the *Uncx4.1*-expressing region is indicated by asterisks. Curly-tail regions of *Zic2 kd/kd* frequently show dorsally restricted bridging of *Uncx4.1* stripes (G, I). ap, anterior compartment of the somite; d, dorsal; pc, posterior compartment of the somite; sb, spina bifida; v, ventral. (J–K) Immunostaining with anti-neurofilament antibody in wild-type (J) and in *Zic2 kd/kd* (K) embryos at E10.5. Arrowheads indicate misrouting of spinal nerve projections from their path. Partial loss of the metameric pattern of the somites are indicated by lines and an asterisk. drg, dorsal root ganglia; scg, sensory chain ganglia; sn, sensory nerve. (L–O) WMISH with *Uncx4.1* RNA probes in E9.75 wild-type (L–M), *Zic3 Bn/Y* (L, N), and *Zic3 Bn/Bn* (L, O) embryos. Restricted and faint staining of *Uncx4.1* is indicated by dashed lines. The difference between (N) and (O) represents a variance generally found in the *Zic3*-null mouse. *Zic3 Bn/Y* and *Zic3 Bn/Bn* were indistinguishable with regard to all embryonic defects. (P–Q) ISH with *Uncx4.1* RNA probes in wild-type (P), and *Zic3 Bn/Y* (Q) in longitudinal sections through lumbar region at E11.5. Fusion of the *Uncx4.1*-expressing region is indicated by asterisk. (T) Lateral views of the tails of wild-type, *Zic2 kd/+*, and *Zic2 kd/kd* mutants at E11.5. Morphologic differences in the tail tips are indicated by asterisks. (U–V) Longitudinal sections through the caudal end of the neural tube in the tail of *Zic2 kd/+* (U) and *Zic2 kd/kd* (V). Abnormal cell cluster extended from the caudal end of the neural tube (white arrowheads). (W) Distribution of Notch1 protein in wild-type, *Zic2 kd/+*, and *Zic2 kd/kd* embryos in longitudinal sections of PSM at E11.5. Notch1 protein (green) is detected in S-1/S0/S1 compartment of PSM. (X–AA) Detection of the activated form of Notch1 protein (NICD) in wild-type (X, Y) and *Zic2 kd/kd* (Z, AA) embryos in longitudinal sections of PSM at E11.5. (X, Z) and (Y, AA) represent the representative two patterns of NICD distribution. Thick red lines indicate areas of enhanced expression of NICD. nt, neural tube; PSM, presomitic mesoderm.

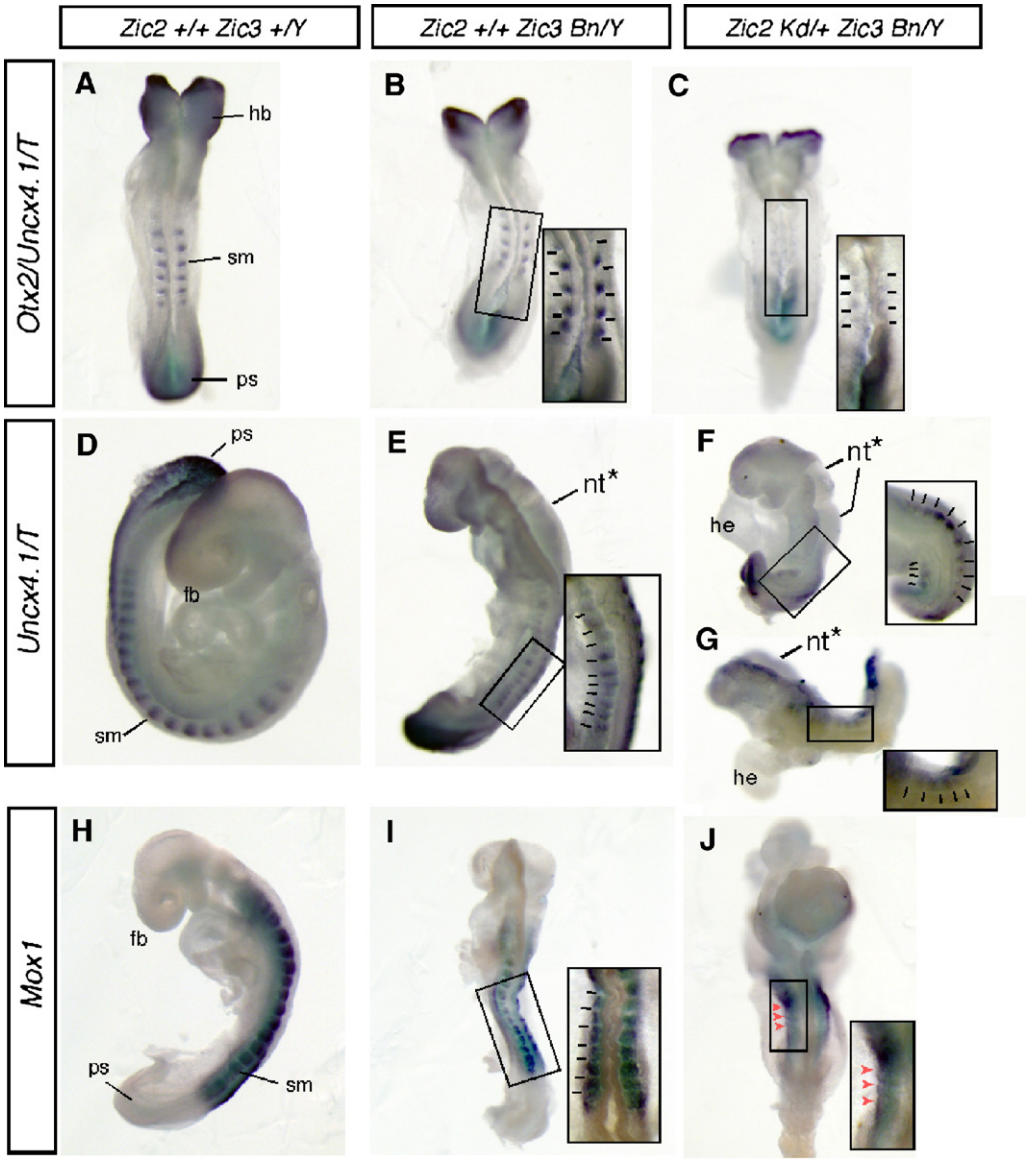

Fig. 7. Early somitic defects in *Zic2*/*Zic3* combined mutant embryos. WMISH was performed in wild-type (*Zic2 +/+ Zic3 +/Y*) (A, D, H), *Zic3 Bn/Y* (*Zic2 +/+ Zic3 Bn/Y*) (B, E, I), and *Zic2 kd/+ Zic3 Bn/Y* (C, F, G, J). Insets indicates higher magnifications of the framed rectangle areas in the same panel. Bars indicate the somite borders. (A–C) WMISH for *Otx2*, *Uncx4.1*, and *Brachyury(T)* at E8.5. (D–G) WMISH for *Uncx4.1* and *Brachyury(T)* at E9.5. Inset in panel F shows dorsal view of framed area of the embryo, indicating bilateral *Uncx4.1* expression. (H–J) WMISH for *Mox1* at E9.5. Arrowheads indicate the irregular and fused expression of Mox1. fb, forebrain; he, heart; nt*, neural tube closure defects; ps, primitive streak; sm, somite.

required for somitogenesis. In E7.5 *Zic2 kd/kd Zic3 Bn/Y* embryos, *Brachyury* staining revealed either a bent path or decreased intensity (Fig. 9H and data not shown), and signals for *Foxa2* (a marker for anterior axial mesoderm; Sasaki and Hogan, 1996; Ang and Rossant, 1994) were weak and detected only in the distal tips of the embryos (Fig. 9I). In addition, anterior neuroectoderm demarcated by *Otx2* (Simeone et al., 1993; Kimura et al., 2000) was reduced in E8.5 *Zic2 kd/+ Zic3 Bn/Y* embryos (Fig. 9F). These findings indicate that a broad range of embryonic patterning was impaired in *Zic2*/*Zic3* compound mutants. However, these defects were essentially similar to those observed in *Zic3* knockout mice (Ware et al., 2006). Except for their roles in segmentation, we find it difficult to conclude unambiguously that Zic2 and Zic3 cooperate in embryonic patterning.

Roles of Zic2 and Zic3 in somitogenesis and mesodermal development

In this study, we analyzed the expression patterns of *Zic2* and *Zic3* during gastrulation to somite stages and somitic defects in *Zic2* single, *Zic3* single, and *Zic2*/*Zic3* compound mutant mice. By analyzing combined mutants, we provide evidence that *Zic2* and *Zic3* exert functional redundancy in mesodermal patterning and somitogenesis. Following observations may be essential to consider the involvement of *Zic2* and

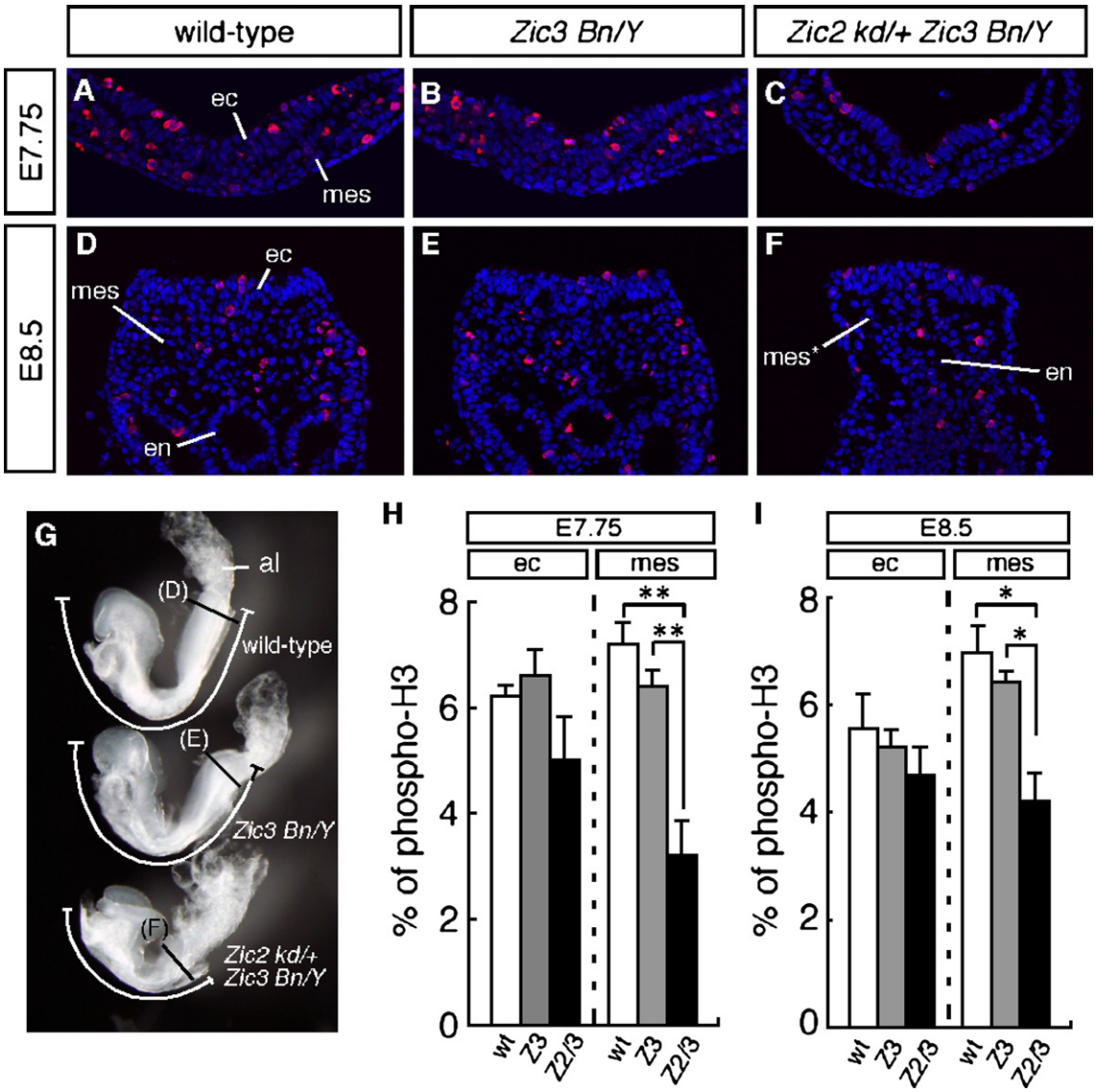

Fig. 8. Cell proliferation in the primitive streak of *Zic2*/*Zic3* combined mutant. (A–F) Transverse sections through primitive streak at E7.75 (A–C) and E8.5 (D–F) in wild-type (A, D), *Zic3 Bn/Y* (B, E) and *Zic2 kd/+ Zic3 Bn/Y* (C, F). Sections were stained with DAPI (blue) and antibodies against phosphohistone H3 (phospho-H3) to detect cells undergoing mitosis (red). Note the decrease in phospho-H3 staining in the mesoderm of the primitive streak. ec, ectoderm; en, endoderm; mes, mesoderm. Reduced number of mesodermal cells in the primitive streak is indicated by asterisk. (G) Representative E8.5 embryos used in the cell proliferation analysis. The rostro-caudal extent of the embryos is shown by curved lines. Section levels for (D–F) are indicated by black lines. al, allantois. (H–I) Percentage of phospho-H3-positive cells in the ectoderm and mesoderm of the primitive streak at E7.75 (H) and E8.5 (I). The results are shown as mean percentage with SEM. $^{*}p<0.05$; $^{**}P<0.01$ by *t*-test. ec, ectoderm; mes, mesoderm.

Zic3 in somite development. (1) *Zic2* and *Zic3* are expressed in the mesoderm and primitive streak region during gastrulation. In somite stages, *Zic2* expression is enhanced in the anterior parts of PSM (in both S0 and S-1) and newly generated somites (S1), whereas *Zic3* is expressed more evenly from S-1 to the tail tip and in segmented somites; (2) The skeletal pattern reveals the segmentation defects, and somite markers occur unevenly along the anterior–posterior in *Zic2* single, *Zic3* single, and *Zic2/Zic3* compound mutants. Subdivision in each somite is more severely impaired in *Zic2 kd/+ Zic3 Bn/Y* and *Zic2 kd/kd Zic3 Bn/Y* compound mutant embryos than in single mutants; (3) Not clear in the single mutant, caudal structures (primitive streak during gastrulation and PSM in later stage) are severely impaired in the *Zic2/Zic3* compound mutant. (4) Early mesodermal patterning through gastrulation is also defective in *Zic2/Zic3* mutants.

In light of these observations, we propose two major roles of *Zic2* and *Zic3* in mesodermal segmentation. The first one is that they maintain somite compartment rather than its specification in the anterior PSM. We first postulated that *Zic2* and *Zic3* could specify somite compartment (i.e. anterior–posterior) at the anterior PSM. However, there were no cases of continuous disappearance of somite regional markers' expression or the disturbance in the anterior PSM markers (*Mesp2*, *EphA4*, and NICD). In addition, somite polarity of newly formed somites was unchanged in *Zic2 kd/kd* embryos. These results suggest

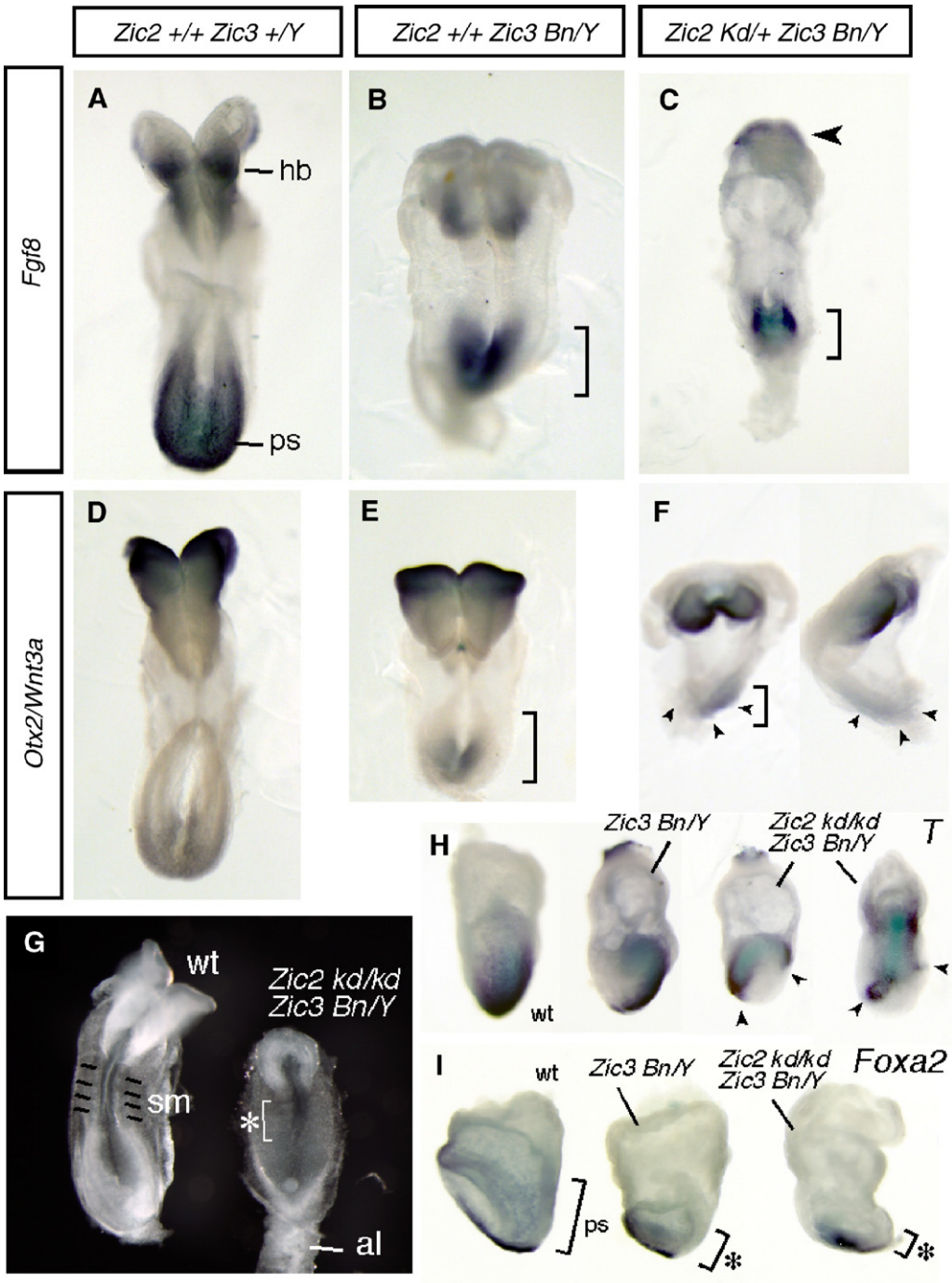

Fig. 9. Mesodermal defects in *Zic2*/*Zic3* combined mutant embryos. Embryos were collected at E7.0–8.5. (A–F) WMISH was performed in wild-type (*Zic2* +/+ *Zic3* +/*Y*) (A, D), *Zic3 Bn/Y* (*Zic2* +/+ *Zic3 Bn/Y*) (B, E), and *Zic2 kd/+ Zic3 Bn/Y* (C, F) embryos. (A–C) WMISH for *Fgf8* was performed at E8.5. hb, hindbrain; ps, primitive streak. Reduced expression of *Fgf8* in the primitive streak region is indicated by the brackets. Hypoplastic anterior structure in *Zic2 kd/+ Zic3 Bn/Y* embryos is indicated by arrowhead. (D–F) WMISH for *Otx2* and *Wnt3a* at E8.5. Dorsal view (left) and lateral view (right) of the *Zic2 kd/+ Zic3 Bn/Y* embryos are shown in (F). Reduced size of *Wnt3a* expression in the primitive streak region is indicated by the brackets. Arrowheads in panel F indicate reduced expression level of *Wnt3a*. (G) Morphology of wild-type (left) and *Zic2 kd/kd Zic3 Bn/Y* (right) embryos at E8.5. Dorsal view of embryos. Poor development of somites in *Zic2 kd/kd Zic3 Bn/Y* embryos is indicated by asterisks. al, allantois; sm, somites. (H) WMISH for *Brachyury(T)* at E7.0. Abnormal expression of *Brachyury* in *Zic2 kd/kd Zic3 Bn/Y*, representing reduced and twisted primitive streak area, is indicated by arrowheads. (I) WMISH for *Foxa2* at E7.5. Reduced primitive streak (ps) areas in *Zic3 Bn/Y* and *Zic2 kd/kd Zic3 Bn/Y* embryos is indicated by asterisks.

that determination of somitic polarity and its border may not directly depend on *Zic2* and *Zic3*. Instead, the primary role for *Zic2* and *Zic3* may be in the maintenance of the somitic integrity by controlling separation of cells and the cell number for formed somite compartments during somite development. Accordingly, segmental disturbance and regional defects of

axial skeletons were also observed in *Zic1* mutant (Aruga et al., 1999), which is expressed later than *Zic2* and *Zic3* in the somitogenesis (Fig. 2E).

The other possible role is that *Zic2* and *Zic3* are required for generation of paraxial mesoderm progenitors from primitive streak and tailbud. It is known that the PSM is constantly supplied caudally with new cells by progenitors located in the primitive streak and tailbud during somitogenesis, and maintenance of PSM size is dependent on these tissues (Tam, 1986; Yamaguchi et al., 1999). We have shown that loss of *Zic2*, *Zic3* or both *Zic2* and *Zic3* lead to a reduction in the body length (total number of generated somites), the size of primitive streak and the PSM. Thus, a reduction of streak- or tailbud-derived progenitors can be an explanation for the axial truncation of in *Zic2, Zic3*, and *Zic2/3* mutants. Taken together with the reduced PSM progenitor cell proliferation in the *Zic2 kd/+ Zic3 Bn/Y* mutant, *Zic2* and *Zic3* may function in the primitive streak and tailbud to control the proliferation of paraxial mesoderm progenitors. The role of *Zic2* and *Zic3* in the regulation of cell proliferation seems to be analogous to the role of Zic genes in other developmental contexts. For example, in cerebella of *Zic1* single and *Zic1/Zic2* combined mutants, cell proliferation of granule neuron progenitor was reduced (Aruga et al., 1998, 2002a), and in spinal cord *Zic1* controls the expansion of neuronal precursors by inhibiting neuronal differentiation (Aruga et al., 2002b). The apparent similarity in the cell proliferation regulation might be related to the functional similarities (i.e. DNA binding property and transcriptional regulation ability) among mouse Zic proteins (Koyabu et al., 2001; Mizugishi et al., 2001).

Our results indicate that *Zic2* and *Zic3* synergistically control multiple steps of mesodermal segmentation in mammals. The abnormality in *Zic1* mutants was most pronounced in the dorsal components of sclerotome-derived structures such as the vertebral arch. Therefore, the subgroup of vertebrate *Zic* genes comprising *Zic1*, *Zic2*, and *Zic3* has a common role in the establishment of metamerism. It is interesting that these three genes strongly preserve some evolutionary conserved domains that are present in the bilateralian ancestor but that have been lost by unsegmented urochordates (Aruga et al., 2006). The redundant and unique functions of *Zic1*, *Zic2*, and *Zic3* may have contributed to the establishment of segmented mesoderm in vertebrates during the course of evolution.

Acknowledgments

We thank Yumiko Saga (National Institute of Genetics) for anti-Mesp2 antibody, Andy McMahon (Harvard University) and Shinji Takada (National Institute for Basic Biology) for *Wnt3a* probe, Peter Gruss (Max-Planck Institute) for *Pax3* probe, Akinori Tokunaga and Hideyuki Okano (Keio University) for helpful advice, and Yayoi Nozaki and RRC RIKEN BSI for technical assistance. This work was supported by a Grant-in-Aid for Scientific Research from the Ministry of Education, Culture, Sports, Science, and Technology of Japan.

Appendix A. Supplementary data

Supplementary data associated with this article can be found, in the online version, at doi:10.1016/j.ydbio.2007.04.003.

References

Ang, S.L., Rossant, J., 1994. HNF-3 beta is essential for node and notochord formation in mouse development. Cell 78, 561–574.

Aruga, J., 2004. The role of *Zic* genes in neural development. Mol. Cell. Neurosci. 26, 205–221.

Aruga, J., Nagai, T., Tokuyama, T., Hayashizaki, Y., Okazaki, Y., Chapman, V.M., Mikoshiba, K., 1996. The mouse *zic* gene family. Homologues of the *Drosophila* pair-rule gene odd-paired. J. Biol. Chem. 271, 1043–1047.

Aruga, J., Minowa, O., Yaginuma, H., Kuno, J., Nagai, T., Noda, T., Mikoshiba, K., 1998. Mouse Zic1 is involved in cerebellar development. J. Neurosci. 18, 284–293.

Aruga, J., Mizugishi, K., koseki, H., Imai, K., Balling, R., Noda, T., Mikoshiba, K., 1999. *Zic1* regulates the patterning of vertebral arches in cooperation with *Gli3*. Mech. Dev. 89, 141–150.

Aruga, J., Inoue, T., Hoshino, J., Mikoshiba, K., 2002a. *Zic2* controls cerebellar development in cooperation with *Zic1*. J. Neurosci. 22, 218–225.

Aruga, J., Tohmonda, T., Homma, S., Mikoshiba, K., 2002b. *Zic1* promotes the expansion of dorsal neural projenitors in spinal cord by inhibiting neuronal differentiation. Dev. Biol. 244, 329–341.

Aruga, J., Ogura, H., Shutoh, F., Ogawa, M., Franke, B., Nagao, S., Mikoshiba, K., 2004. Locomotor and oculomotor impairment associated with cerebellar dysgenesis in *Zic3*-deficient (*Bent tail*) mutant mice. Eur. J. Neurosci. 20, 2159–2167.

Aruga, J., Kamiya, A., Takahashi, H., Fujimi, T.J., Shimizu, Y., Ohkawa, K., Yazawa, S., Umesono, Y., Noguchi, H., Shimizu, T., Saitou, N., Mikoshiba, K., Sakaki, Y., Agata, K., Toyoda, A., 2006. A wide-range phylogenetic analysis of Zic proteins: implications for correlations between protein structure conservation and body plan complexity. Genomics 87, 783–792.

Aulehla, A., Herrmann, B.G., 2004. Segmentation in vertebrates: clock and gradient finally joined. Genes Dev. 18, 2060–2067.

Brown, S.A., Warburton, D., Brown, L.Y., Yu, C.Y., Roeder, E.R., Stengel-Rutkowski, S., Hennekam, R.C., Muenke, M., 1998. Holoprosencephaly due to mutations in *ZIC2*, a homologue of *Drosophila* odd-paired. Nat. Genet. 20, 180–183.

Brown, L.Y., Kottmann, A.H., Brown, S., 2003. Immunolocalization of *Zic2* expression in the developing mouse forebrain. Gene Expr. Patterns 3, 361–367.

Burgess, R., Cserjesi, P., Ligon, K.L., Olson, E.N., 1995. Paraxis: a basic helix–loop–helices protein expressed in paraxial mesoderm and developing somites. Dev. Biol. 168, 296–306.

Bussen, M., Petry, M., Schuster-Gossler, K., Leitges, M., Gossler, A., Kispert, A., 2004. The T-box transcription factor *Tbx18* maintains the separation of anterior and posterior somite compartments. Genes Dev. 18, 1209–1221.

Candia, A.F., Hu, H., Crosby, J., Lalley, P.A., Noden, D., Nadeau, J.H., Wright, C.V.E., 1992. *Mox1* and *Mox2* define a novel homeobox gene subfamily and are differently expressed during early mesodermal patterning in mouse embryos. Development 116, 1123–1136.

Carrel, T., Purandare, S.M., Harrison, W., Elder, F., Fox, T., Casey, B., Herman, G.E., 2000. The X-linked mouse mutation *Bent tail* is associated with a deletion of the *Zic3* locus. Hum. Mol. Genet. 9, 1937–1942.

Deutsch, U., Dressler, G.R., Gruss, P., 1991. *Pax1*, a member of a paired box homologous murine gene family, is expressed in segmented structures during development. Cell 53, 617–625.

Dodd, J., Morton, S.B., Karagogeos, D., Yamamoto, M., Jessell, T.M., 1988. Spatial regulation of axonal glycoprotein expression on subsets of embryonic spinal neurons. Neuron 1, 105–116.

Downs, K.M., Davies, T., 1993. Staging of gastrulating mouse embryos by morphological landmarks in the dissecting microscope. Development 118, 1255–1266.

Dubrulle, J., Pourquie, O., 2004. Coupling segmentation to axis formation. Development 131, 5783–5793.

Dubrulle, J., McGrew, M.J., Pourquie, O., 2001. FGF signaling controls somite boundary position and regulates segmentation clock control of spatiotemporal *Hox* gene activation. Cell 106, 219–232.

Elms, P., Siggers, P., Napper, D., Greenfield, A., Arkell, R., 2003. *Zic2* is required for neural crest formation and hindbrain patterning during mouse development. Dev. Biol. 264, 391–406.

Elms, P., Scurry, A., Davies, J., Willoughby, C., Hacker, T., Bogani, D., Arkell, R., 2004. Overlapping and distinct expression domains of *Zic2* and *Zic3* during mouse gastrulation. Gene Expr. Patterns 4, 505–511.

Franke, B., Klootwijk, R., Hekking, J.W., de Boer, R.T., ten Donkelaar, H.J., Mariman, E.C., van Straaten, H.W., 2003. Analysis of embryonic phenotype of *Bent tail*, a mouse model for X-linked neural tube defects. Anat. Embryol. 207, 255–262.

Galceran, J., Sustmann, C., Hsu, S.C., Folberth, S., Grosschedl, R., 2004. LEF1-mediated regulation of Delta-like1 links Wnt and Notch signaling in somitogenesis. Genes Dev. 18, 2718–2723.

Garber, E.D., 1952. "*Bent tail*," a dominant, sex-linked mutation in the mouse. Proc. Natl. Acad. Sci. 38, 876–879.

Gebbia, M., Ferrero, G.B., Pilia, G., Bassi, M.T., Aylsworth, A., Penman-Splitt, M., Bird, L.M., Bamforth, J.S., Burn, J., Schlessinger, D., Nelson, D.L., Casey, B., 1997. X-linked situs abnormalities result from mutations in *ZIC3*. Nat. Genet. 17, 305–308.

Goulding, M.D., Georges Chalepakis, G., Deutsch, U., Join R.Erselius, J.E., Gruss, P., 1991. Pax-3, a novel murine DNA binding protein expressed during early neurogenesis. EMBO J. 10, 1135–1147.

Goulding, M., Andrew Lumsden, A., Paquette, A., 1994. Regulation of Pax-3 expression in the dermomyotome and its role in muscle development. Development 120, 957–971.

Grinberg, I., Millen, K.J., 2005. The *ZIC* gene family in development and disease. Clin. Genet. 67, 290–296.

Herman, G.E., El-Hodiri, H.M., 2002. The role of *ZIC3* in vertebrate development. Cytogenet. Genome Res. 99, 229–235.

Herrera, E., Brown, L.Y., Aruga, J., Mikoshiba, K., Rachel, R.A., Dolen, G., Brown, S., Mason, C.A., 2003. The transcription factor *Zic2* designates the uncrossed retinal ganglion cell axon projection. Cell 114, 545–557.

Hofman, M., Schuster-Gossler, K., Watanabe-Rudolph, M., Aulehla, A., Herrmann, B.G., Gossler, A., 2004. WNT signaling, in synergy with T/TBX6, controls Notch signaling by regulating *Dll1* expression in the presomitic mesoderm of mouse embryos. Genes Dev. 18, 2712–2717.

Hogan, B., Beddington, R., Constantini, F., Lacy, E. (Eds.), 1994. Staining Embryos for Cartilage and Bone. Manipulating the Mouse Embryo. Cold Spring Harbor Laboratory Press, New York, pp. 379–380.

Holley, S.A., Takeda, H., 2002. Catching a wave: the oscillator and wavefront that create the zebrafish somite. Semin. Cell Dev. Biol. 13, 481–488.

Inoue, T., Hatayama, M., Tohmonda, T., Itohara, S., Aruga, J., Mikoshiba, K., 2004. Mouse *Zic5* deficiency results in neural tube defects and hypoplasia of cephalic neural crest derivatives. Dev. Biol. 270, 146–162.

Kawamura, A., Koshida, S., Hijikata, H., Sakaguchi, T., Kondoh, H., Takada, S., 2005. Zebrafish *Hairy/Enhancer* of split protein links FGF signaling to cyclic gene expression in the periodic segmentation of somites. Genes Dev. 19, 1156–1161.

Kimura, C., Yoshinaga, K., Tian, E., Suzuki, M., Aizawa, S., Matsuo, I., 2000. Visceral endoderm mediates forebrain development by suppressing posteriorizing signals. Dev. Biol. 225, 304–321.

Klootwijk, R., Franke, B., van der Zee, C.E., de Boer, R.T., Wilms, W., Hol, F. A., Mariman, E.C., 2000. A deletion encompassing *Zic3* in *bent tail*, a mouse model for X-linked neural tube defects. Hum. Mol. Genet. 9, 1615–1622.

Koyabu, Y., Nakata, K., Mizugishi, K., Aruga, J., Mikoshiba, K., 2001. Physical and functional interactions between Zic and Gli proteins. J. Biol. Chem. 276, 6889–6892.

Kraus, F., Haenig, B., Kispert, A., 2001. Cloning and expression analysis of the mouse T-box gene *Tbx18*. Mech. Dev. 100, 83–86.

Maroto, M., Pourquie, O., 2001. A molecular clock involved in somite segmentation. Curr. Top. Dev. Biol. 51, 221–248.

Mizugishi, K., Aruga, J., Nakata, K., Mikoshiba, K., 2001. Molecular properties of Zic proteins as transcriptional regulators and their relationship to GLI proteins. J. Biol. Chem. 276, 2180–2188.

Mizugishi, K., Hatayama, M., Tohmonda, T., Ogawa, M., Inoue, T., Mikoshiba, K., Aruga, J., 2004. Myogenic repressor I-mfa interferes with function of Zic family proteins. Biochem. Biophys. Res. Comm. 320, 233–240.

Morimoto, M., Takahashi, Y., Endo, M., Saga, Y., 2005. The *Mesp2* transcription factor establishes segmental borders by suppressing Notch activity. Nature 435, 354–359.

Nagai, T., Aruga, J., Takada, S., Gunther, T., Sporle, R., Schughart, K., Mikoshiba, K., 1997. The expression of the mouse *Zic1*, *Zic2*, and *Zic3* gene suggests an essential role for *Zic* genes in body pattern formation. Dev. Biol. 182, 299–313.

Nagai, T., Aruga, J., Minowa, O., Sugimoto, T., Ohno, Y., Noda, T., Mikoshiba, K., 2000. *Zic2* regulates the kinetics of neurulation. Proc. Natl. Acad. Sci. U. S. A. 97, 1618–1623.

Nakajima, Y., Morimoto, M., Takahashi, Y., Koseki, H., Saga, Y., 2006. Identification of Epha4 enhancer required for segmental expression and the regulation by *Mesp2*. Development 133, 2517–2525.

Nieto, M.A., Gilardi-Hebenstreit, P., Charnay, P., Wilkinson, D.G., 1992. A receptor protein tyrosine kinase implicated in the segmental patterning of the hindbrain and mesoderm. Development 116, 1137–1150.

Pourquie, O., 2003. The segmentation clock: converting embryonic time into spatial pattern. Science 301, 328–330.

Purandare, S.M., Ware, S.M., Kwan, K.M., Gebbia, M., Bassi, M.T., Deng, J.M., Vogel, H., Behringer, R.R., Belmont, J.W., Casey, B., 2002. A complex syndrome of left–right axis, central nervous system and axial skeleton defects in *Zic3* mutant mice. Development 129, 2293–2302.

Rida, P.C., Le Minh, N., Jiang, Y.J., 2004. A Notch feeling of somite segmentation and beyond. Dev. Biol. 265, 2–22.

Saga, Y., Takeda, H., 2001. The making of the somite: molecular events in vertebrate segmentation. Nat. Rev. Genet. 2, 835–845.

Saga, Y., Hata, N., Koseki, H., Taketo, M.M., 1997. *Mesp2*: a novel mouse gene expressed in the presegmented mesoderm and essential for segmentation initiation. Genes Dev. 11, 1827–1839.

Sasaki, H., Hogan, B.L., 1996. Enhancer analysis of the mouse HNF-3 beta gene: regulatory elements for node/notochord and floor plate are independent and consist of multiple sub-elements. Genes Cells 1, 59–72.

Simeone, A., Acampora, D., Mallamaci, A., Stornaiuolo, A., D'Apice, M.R., Nigro, V., Boncinelli, E., 1993. A vertebrate gene related to orthodenticle contains a homeodomain of the bicoid class and demarcates anterior neuroectoderm in the gastrulating mouse embryo. EMBO J. 12, 2735–2747.

Takada, S., Stark, K.L., Shea, M.J., Vassileva, G., McMahon, J.A., McMahon, A.P., 1994. Wnt-3a regulates somite and tailbud formation in the mouse embryo. Genes Dev. 8, 174–189.

Takahashi, Y., Koizumi, K., Takagi, A., Kitajima, S., Inoue, T., Koseki, H., Saga, Y., 2000. *Mesp2* initiates somite segmentation through the Notch signaling pathway. Nat. Genet. 25, 390–396.

Tam, P.P., 1986. A study of the pattern of prospective somites in the presomitic mesoderm of mouse embryos. J. Embryol. Exp. Morphol. 92, 269–285.

Tokunaga, A., Kohyama, J., Yoshida, T., Nakao, K., Sawamoto, K., Okano, H., 2004. J. Neurochem. 90, 142–154.

Ware, S.M., Harutyunyan, K.G., Belmont, J.W., 2006. *Zic3* is critical for early embryonic patterning during gastrulation. Dev. Dyn. 235, 776–785.

Yamaguchi, T.P., Bradley, A., McMahon, A.P., Jones, S., 1999. A Wnt5a pathway underlies outgrowth of multiple structures in the vertebrate embryo. Development 126, 1211–1223.